Practice research of comprehensive and quantitative autoantibody assay systems

自己抗体バイオマーカーの網羅的定量評価システムの実用化研究

2023, March

Ai Miyamoto

Graduate School of Interdisciplinary

Science and Engineering in Health Systems

(Doctor’s Course)

OKAYAMA UNIVERSITY

Contents

GENERAL INTRODUCTION

1. Introduction to cancer immunotherapy

The "immune system" plays a critical role in protecting the body from bacterial or viral infections or other foreign substances in the human body. This immune system also contributes to the elimination of abnormal cancer cells. Recent immune oncological studies reveal that clinically observed human cancer gains function to escape immunological elimination [1-4]. The clinical trials to activate the antitumor immune responses have been lengthy trials by many clinicians. In the 1890s, Dr. William Coley hypothesized that bacterial infection triggers antitumor immunity [5, 6]. It has been reported that many cancer patients showed successful tumor regressions by intratumoral administration of Coly's toxin, composing filtrated fractions from killed bacteria of species Streptococcus pyogenes and Serratia marcescens. Although Coly's toxin has been employed as an alternative medicine for a long time, this concept might be historically too early in an immature immunological science period. With increased interest in chemotherapy or radiotherapy, Coly's toxin was buried in history for a while. Subsequent research trends of immune-oncology moved to an extracellular protein of cytokines that induce immune responses [6]. Administration of cytokine in cancer patients expected to upregulate tumor immunity, but failed to show efficacy in many cancers. In 21-century, along with an understanding of the mechanism of immune-oncology, various cancer immune therapy was proposed, including dendritic cell therapy, cancer peptide vaccine, humanized antibody-based therapy, natural killer T cell therapy (NKT therapy), gamma-delta (γδ) T cell therapy [6]. However, none of these treatments have yet overcome cancer. One of the critical reasons is clinically recognized tumors developed as heterogenous cell mixtures with the ability to evade immune cell attack [7, 8]. Nevertheless, the efficacy of cancer immunotherapy has been steadily increasing with the advent of immune checkpoint inhibitors (ICIs), which unlock the immune escape mechanism of these troublesome cancer cells.

2. Innate and acquired immune system

The human immune system can categorize into two types: innate immunity and acquired immunity. Innate immunity is the mechanism we are born with to eliminate foreign substances. Acquired immunity is an antigen-specific immune response induced against a foreign substance. In this reaction, dendritic cells (DCs) phagocytose bacterial or viral

foreign substances, or abnormal proteins in cancer cells referred to as cancer antigens, then present their peptide antigens on major histocompatibility complex (MHC) molecules [1]. Namely, cancer antigens are critical targets for antitumor immune reactions. Antigen peptides on MHC class I induces cellular immunity, then CD8+ cytotoxic T-cells attack antigen peptide-presented cells, e.g., tumor cells [9]. Antigen peptides on MHC class II induce antigen-specific Immunoglobulin (Ig) proteins called humoral immunity. CD4+ helper T cells recognized the peptide antigens presented on the MHC class II of DCs; helper T cells are activated and proliferate by cytokine secretion. CD4+ helper T cells regulate the production of antigen-specific Immunoglobulin (Ig) proteins. For example, antigen molecules leaked from dead cancer cells, uptake into cells by binding to antigen-specific membrane-bound immunoglobulin M (IgM) of B cells and are then presented as antigen peptides on the MHC class II. When the CD4+ helper T cells recognize target antigens on B-cells, these B cells differentiate into antibody-producing plasma cells, which induces a class switch to produce IgG antibodies. This immune response is called humoral immunity; cancer antigens also associate with this immunity cycle (Figure 1).

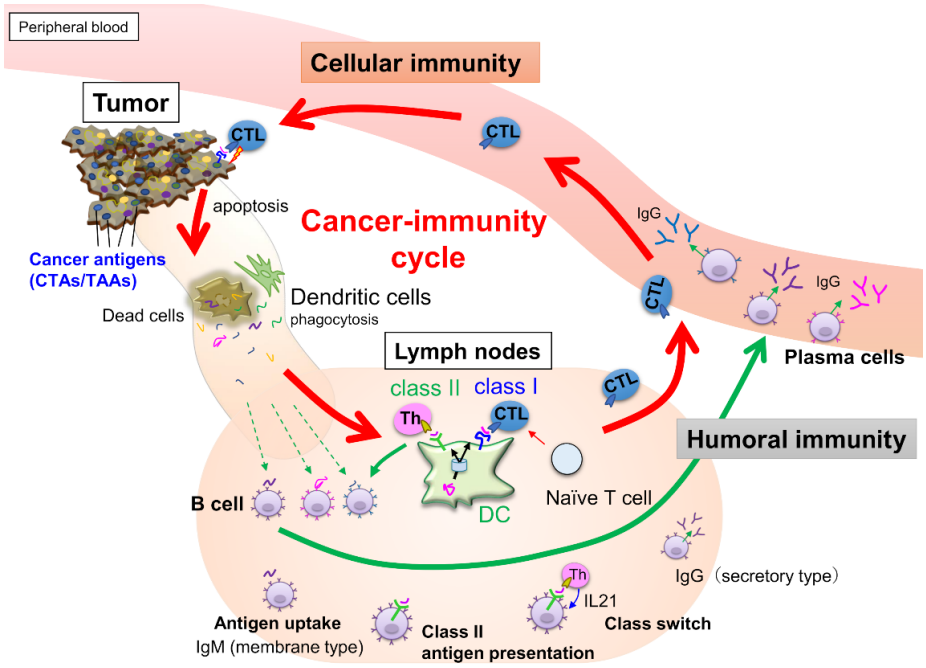

Figure 1 Schematic of acquired immunity in cancer.

Cancer antigens recognized as foreign induce cellular and humoral immunity. In humoral immunity, antigen-specific Ig proteins are induced. In cellular immunity, cancer antigens taken up by dendritic cells are presented as peptides on MHC molecules, and CD8+ cytotoxic T-cells attack tumor cells presenting these peptides.

3. Tumor microenvironment

The immune system can eliminate cancer cells by recognizing cancer antigens expressed in malignant cells. This cancer immunosurveillance concept is now clearly described by a seven-step cancer immunity cycle (Figure 2) [10]. In the first step, are released antigens from dead cells (step 1). DCs present the captured antigens on MHCI and MHCII molecules to T cells (step 2). Antigen-specific T cells are activated by antigen presentation of DCs (step 3). The activated effector T cells traffic to (step 4) and infiltrated the tumor bed (step 5). T cells recognize cancer cells expressing cancer antigens (step 6) and kill their target cancer cell (step 7). The killing of the cancer cell releases additional tumor-associated antigens (step 1 again). Cancer cells are thought to escape from immune surveillance mechanisms when any action in this cycle is impaired.

In addition, a new concept of "cancer immunoediting" has emerged (Figure 3) [4]. Cancer immunoediting consists of three phases: elimination, equilibrium, and escape. In the elimination phase, innate and acquired immunity kills cancer cells long before the tumor is clinically evident. Suppose the cells did not kill in the elimination, the phase transitions to equilibration. In the equilibration phase, the cancer-immune system prevents the proliferation of cancer cells. Some cancer cells develop new mutations making them resistant to the immune system's attack in this phase. Then, cancer cell variants emerge as (i) cells that are no longer recognized by the immune system due to antigen loss mutants or defects in antigen processing and presentation, (ii) cells that are insensitive to immune effector functions, and (iii) cells that cause immunosuppressive conditions in the cancer microenvironment. Then, these cells transition to the escape phase. Tumor variants that have become unsusceptible to the immune attacks extend in an unrestrained pattern in this phase. As a result, immunologically carved tumors expand steadily and become clinically evident. The immunogenicity of cancer cells is determined by antigen peptides present on MHC class I. Cancer antigens can be classified into two groups: aberrantly expressed tumor-associated antigens (TAAs) [11] and cancer/testis antigens (CTAs) [12-14], or neoantigens derived from mutated gene products [15, 16]. TAAs and CTAs categorize shared antigens that are universally detectable in different patients. In contrast, somatic mutation-derived neoantigens show patient-specific individual variations [17]. Not all the TAA- or CTA-derived peptides can be present on MHC class I. However, these aberrantly expressed antigens could be involved in the humoral immune response. Hence, serum autoantibodies to cancer antigens reflect the current immune response level associated with tumor volume and antigenicity. The activation of the antitumor immune response is accompanied by an increase in the number

of autoantibodies against various cancer antigens [18-24], referred to as antigen spreading, which could be a critical pharmacodynamic biomarker for the clinical outcome of cancer immunotherapy [20, 24-27]. Accumulating evidence indicates that antibody-antigen immune complex uptake through Fcγ receptors on antigen-presenting cells induces cross-presentation, stimulating long-term antitumor cellular immunity [28].

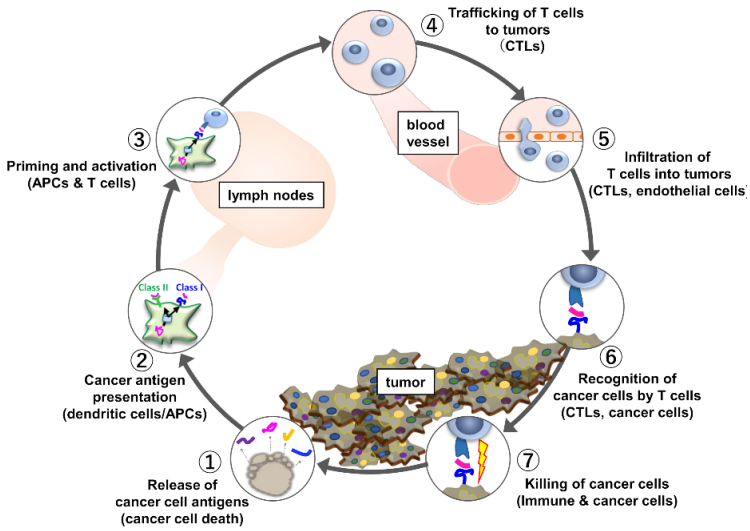

Figure 2 Cancer immunity cycle.

The immune response to cancer is viewed as a series of cycles consisting of seven-steps. Inhibition of any step makes induction of an effective cancer immune response difficult.

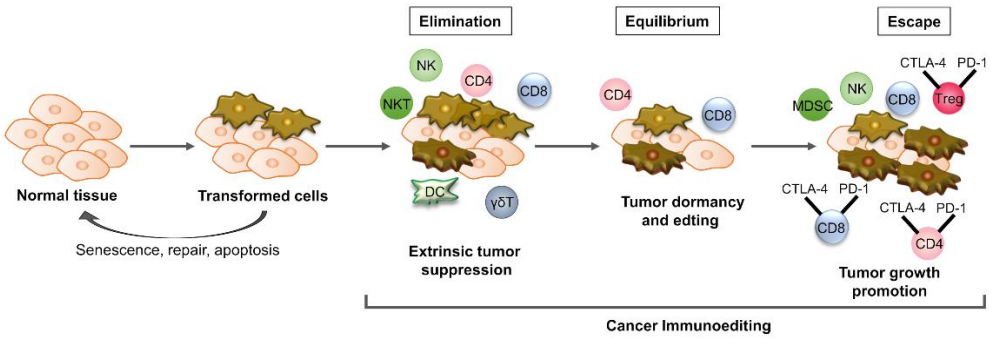

Figure 3 Cancer immunoediting.

Cancer immunoediting consists of three phases: elimination, equilibrium, and escape. In the elimination phase, tumor cells are killed by innate and acquired immunity. In the equilibrium phase, acquired immunity prevents cancer cells from proliferating. Editing of tumor immunogenicity occurs in the equilibrium phase. In the escape phase, the growth of tumor cells that cannot be eliminated by acquired immunity is promoted. These tumor cells emerge to cause clinically apparent disease. NKT, natural killer T-cell; NK, natural killer cell; DC, dendritic cell; γδT, γδT cell; MDSC, Myeloid-derived suppressor cells; Treg, regulatory T cell.

4. Cancer/testis antigens

CTAs is an antigen expressed only in the testis (and placenta) in normal tissues and various cancer cells in tumor tissues [12-14]. Many of the antigens are highly immunogenic. CTAs are now considered attractive targets for cancer immunotherapy [12-14]. Many recombinant CTAs appear to show an aggregation-favored unstable property [29]. This property is consistent with the bioinformatics prediction of the structure of CTAs, which shows that the majority of CTAs are intrinsically disordered proteins (IDPs) [30]. These IDPs, or IDP regions, lack rigid tertiary structures under physiological conditions in vitro; however, they can fold after binding to target macromolecules in vivo [31]. Thus, recombinant CTA proteins in a disordered conformation frequently form inclusion bodies in host cells [32]. The expression pattern, antigenicity, and epitope of cancer antigens differ in each individual [25, 33, 34]. We prepare purified water-soluble and full-length antigens using cysteine sulfhydryl group cationization (S-cationization) chemistry [35-37].

5. Immune checkpoint inhibitors

Immune checkpoint inhibitors (ICIs) inhibit molecules that suppress the immune response. ICIs include anti-PD-1, anti-PD-L1and anti-CTLA-4 (Figure 4)[38, 39]. CTLA-4 is the molecule that inactivates T cells in step 3 of the cancer immunity cycle (Figure 3). PD-1 and PD-L1 are the molecules that inactivate T cells in steps 3 and 7 of the cancer immunity cycle. Anti-PD-1 antibodies bind to PD-1 on T cells and inhibit the binding of PD-1 to PD-L1/PD-L2, blocking the transmission of inhibitory signals, maintaining T cell activation, and restoring antitumor effects. PD-L1 is a ligand for PD-1 expressed on cancer cells. Anti-PD-L1 antibodies inhibit the interaction with PD-1 on T cells by binding to PD-L1 expressed by cancer cells and antigen-presenting cells. As a result, inhibitory signaling to T cells is blocked, and T cell activation is maintained. ICIs have shown better clinical response than conventional cancer therapies (surgery, chemotherapy, and radiation therapy) in some patients and have become one of the reliable treatment options that can prolong life [40].

On the other hand, their clinical responses vary from patient to patient due to the complexity of tumor-immune interactions [41]. Different steps in the cancer-immunity cycle by which tumors escape immunosurveillance are likely to differ among patients [42, 43]. In addition, autoimmune disease may be induced as a side effect in some cancer patients because cancer immunity and autoimmunity are paper thin [44, 45]. Therefore, cancer immunotherapy needs to be personalized to identify the rate-limiting steps in

individual patients, and a combination of strategies should be used to overcome these hurdles.

The significant individual differences in response rates are because each patient has a different immune status from cancer to cancer. Cancer cells can be broadly classified into hot and cold tumors based on tumor immunology [46]. Hot tumors respond to ICI because of their high antigenicity and the ability of immune cells to infiltrate cancer cells. On the other hand, cold tumors do not respond to ICI due to low antigenicity and immune cell exhaustion. These are evidenced by direct confirmation of tumor status by biopsy, including tumor PD-L1 expression (TPS), tumor mutation burden (TMB), and microsatellite instability (MSI) [47-49]. However, these techniques present challenges, such as high invasiveness and heterogeneity within the tumor. Therefore, there is a need for a method to confirm the status of tumors using liquid biopsy with body fluids.

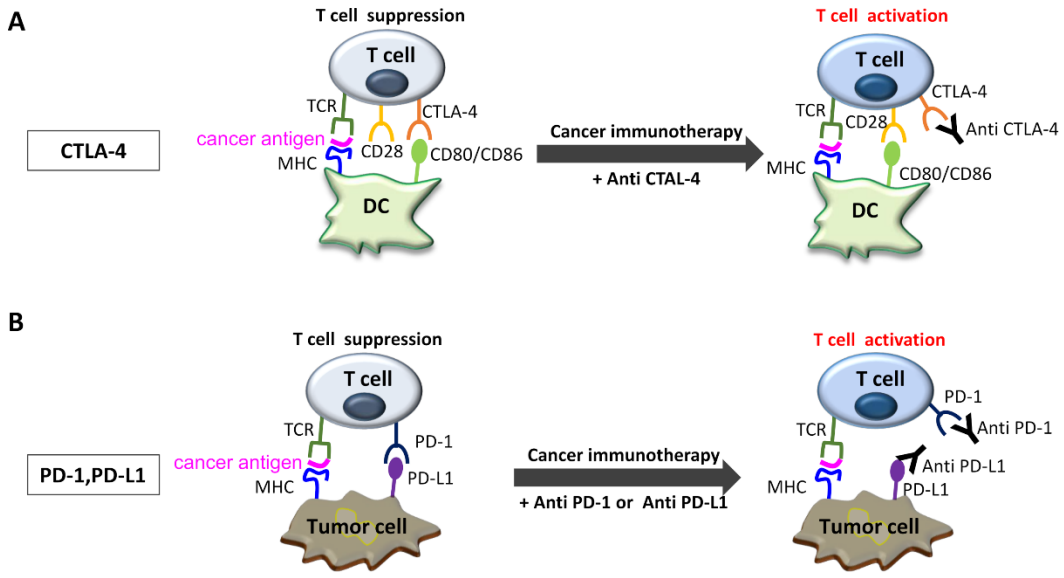

Figure 4 Schematic drawing of the molecular mechanism of immune checkpoint inhibitor.
(A) CTLA-4 suppresses T cells activation by binding to CD80 or CD86. Anti-CTLA-4 activates T cells by inhibiting the CTLA-4/CD80 or CTLA-4/CD86 interaction.
(B) T cell activation is inhibited by the interaction between PD-1 on T cells and PD-L1 on tumor cells. Anti-PD-1 and anti-PD-L1 activate T cells by inhibiting the PD-1/PD-L1 interaction.

6. Purpose of this study

We focused on autoantibodies against cancer antigens, such as TAAs or CTAs, as biomarkers to predict the clinical response of ICI. In general, in addition to the conventional enzyme-linked immunosorbent assay (ELISA) approaches, protein microarray and multiplex bead techniques have been applied to measure antibodies to TAAs or CTAs. Since the expression pattern, antigenicity, epitope, etc., of cancer antigens differ from person to person, the evaluation of cancer immune response using autoantibodies must be comprehensive [25, 33, 34]. To quantitatively evaluate antigen spreading, we designed a multiple *S*-cationized antigen-immobilized bead array (MUSCAT) assay system. Monitoring antigen spreading by the level of autoantibody biomarker requires validated positive control to ensure diagnostic accuracy. The study was conducted to determine if water-soluble reversible *S*-cationized antigen could be used both as an antigen recognized by serum antibodies in the MUSCAT assay and as an antigen to immunize rabbits to obtain antibody-positive controls (Chapter 1).

Furthermore, to prove the MUSCAT-assay's clinical usefulness, Beads validation and Assay validation for the measurement are necessary. In this study, we addressed the development of these validation methods (Chapter 2).

Chapter1 Engineering Cancer/Testis Antigens with Reversible S-Cationization to Evaluate Antigen Spreading

Abstract

Serum autoantibody to cancer/testis antigens (CTAs) is a critical biomarker that reflects the antitumor immune response. Quantitative and multiplexed anti-CTA detection arrays can assess the immune status in tumors and monitor therapy-induced antitumor immune reactions. Most full-length recombinant CTA proteins tend to aggregate. Cysteine residue-specific *S*-cationization techniques facilitate the preparation of water-soluble and full-length CTAs. Combined with Luminex technology, we designed a multiple *S*-cationized antigen-immobilized bead array (MUSCAT) assay system to evaluate multiple serum antibodies to CTAs. Reducible *S*-alkyl-disulfide-cationized antigens in cytosolic conditions were employed to develop rabbit polyclonal antibodies as positive controls. These control antibodies sensitively detected immobilized antigens on beads and endogenous antigens in human lung cancer-derived cell lines. Rabbit polyclonal antibodies successfully confirmed the dynamic ranges and quantitative MUSCAT assay results. An immune monitoring study was conducted using the serum samples on an adenovirus−mediated REIC/Dkk−3 gene therapy clinical trial that showed a successful clinical response in metastatic castration-resistant prostate cancer. Autoantibody responses were closely related to clinical outcomes. Notably, upregulation of anti-CTA responses was monitored before tumor regression. Thus, quantitative monitoring of anti-CTA antibody biomarkers can be used to evaluate the cancer-immunity cycle. A quality-certified serum autoantibody monitoring system is a powerful tool for developing and evaluating cancer immunotherapy.

Introduction

Growing evidence shows that many patients with cancer benefit from immunotherapy [40]. The immune system can eliminate cancer cells by recognizing cancer antigens expressed in malignant cells. This cancer immunosurveillance concept is now clearly described by a seven-step cancer immunity cycle [10]. Most cancers adopt strategies to evade the immune system after a long struggle between malignant cells and the immune system [1-3]. Thus, reactivation of the antitumor immune response and upregulation of the cancer-immunity cycle are critical to ensure improved clinical response. Immune checkpoint inhibitors are currently the most promising treatment for upregulating the

cancer-immunity cycle; however, their clinical responses vary from patient to patient due to the complexity of tumor-immune interactions [41] . Recent analysis of the mechanisms of immune suppression in cancer revealed that different steps in the cancer-immunity cycle by which tumors escape immunosurveillance are likely to differ among patients [42, 43]. Therefore, cancer immunotherapy needs to be personalized to identify the rate-limiting steps in individual patients, and a combination of strategies should be used to overcome these hurdles. To realize personalized precision cancer immune therapy, a technique that can monitor the cancer-immunity cycle will be a powerful tool for treatment.

The immunogenicity of cancer cells is determined by antigen peptides present on MHC class I, and CD8+ cytotoxic lymphocytes eliminate cells by recognizing this complex [9]. Cancer antigens can be classified into two groups: aberrantly expressed tumor-associated antigens (TAAs) [11] and cancer/testis antigens (CTAs) [12, 13], or neoantigens derived from mutated gene products [15, 16]. Both TAAs and CTAs are known as shared antigens that are universally detectable in different patients. In contrast, somatic mutation-derived neoantigens show patient-specific individual variations [17].

During the cancer-immunity cycle activation, antigens released from cancer cells are then captured by dendritic cells, but not all the TAA- or CTA-derived peptides can present on MHC class I. However, these aberrantly expressed antigens could be involved in the humoral immune response. Hence, serum autoantibodies to cancer antigens reflect the current immune response level associated with tumor volume and antigenicity (Figure 1-1). Once cancer cells are destroyed, many cancer antigens are released from them, captured by antigen-presenting cells, and induce T and B cell immune responses. The activation of the antitumor immune response is accompanied by an increase in the number of autoantibodies against various cancer antigens, referred to as antigen spreading [18-24] which could be a critical pharmacodynamic biomarker for the clinical outcome of cancer immunotherapy [20, 24-27]. Accumulating evidence indicates that antibody-antigen immune complex uptake through Fcγ receptors on antigen-presenting cells induces cross-presentation, stimulating long-term antitumor cellular immunity [28]. Thus, a simple blood test-based evaluation of antigen spreading with cancer-immunity cycle activation could predict systemic cancer immunity.

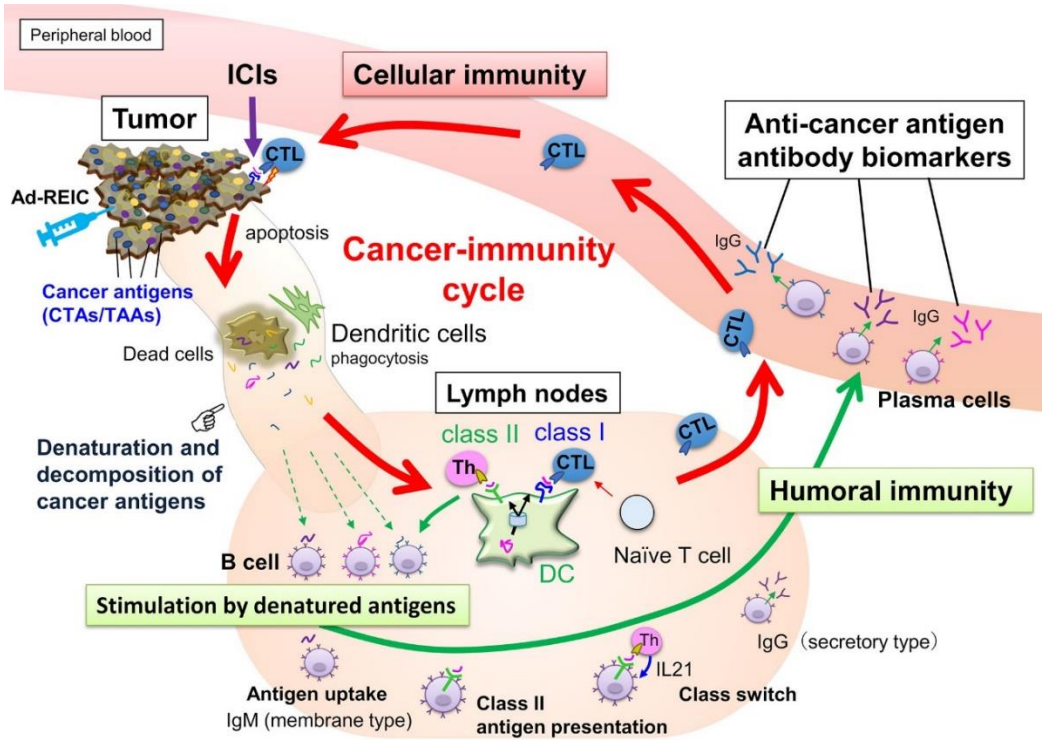

Figure 1-1 Anticancer immunity is enhanced by the cancer-immunity cycle, and cytotoxic T-lymphocytes (CTLs) eliminate cancer cells.

Along with activating the cancer-immunity cycle, antibodies against cancer antigens upregulate by stimulation of released antigens from the cancer cells. Most intracellular cancer antigens suggest easy to denature and decompose after release from cancer cells due to their unstable physical properties. Antibody-producing cells that bind to denatured cancer antigens proliferate, so anti-cancer antigen IgGs recognizing the amino acid sequence of linear epitopes increase preferentially.

The diagnosable set of cancer antigens requires a comprehensive array because the expression pattern, antigenicity, and epitopes vary in individual patients [25, 33, 34]. Full-length cancer antigen preparation is favored for monitoring antigen spreading based on these requirements. However, many recombinant CTAs appear to show an aggregation-favored unstable property [29]. This property is consistent with the bioinformatics prediction of the structure of CTAs, which shows that the majority of CTAs are intrinsically disordered proteins (IDPs) [30]. These IDPs, or IDP regions, lack rigid tertiary structures under physiological conditions in vitro; however, they can fold after binding to target macromolecules in vivo [31]. Thus, recombinant CTA proteins in a disordered conformation frequently form inclusion bodies in host cells [32].

In order to quantitatively evaluate antigen spreading, we designed a multiple *S*-cationized antigen-immobilized bead array (MUSCAT) assay system [32]. *S*-

cationization techniques are employed as a powerful solubilization tool by conjugation of cationic moieties in sulfhydryl groups in denatured protein [35-37]. Full-length and water-soluble *S*-cationized antigens were covalently immobilized onto Luminex magnetic beads via the activated carboxylic acid of the COOH radical group [32, 50]. Although immobilized *S*-cationized antigen on beads modified all Cys residues and limited amino-groups employed for immobilization, specific antibodies raised in cancer patients were quantitatively detected by the Luminex assay with high sensitivity. This MUSCAT assay system can detect polyclonal antibodies recognizing the linear epitope. Epitope-mapping study of anti-CTA autoantibodies in patient sera revealed that these antibodies are polyclonal and recognize individually different linear epitopes [33]. Most CTAs are predicted to have no rigid ordered conformation [30], so antibodies recognizing conformational epitopes are most likely rare. Furthermore, recent knowledge-based and in silico analyses of linear epitopes showed that Cys is a minor frequent amino acid residue [51]. Chemically modified Cys has minimal effect on the antibody binding efficiency. Thus, the MUSCAT assay system is a powerful strategy for quantifying antigen spreading to diagnose cancer immunotherapy.

Monitoring antigen spreading by the level of autoantibody biomarker requires validated positive control to ensure diagnostic accuracy. This study demonstrated that water-soluble reversibly *S*-cationized CTAs can be employed in both antigens recognized by serum antibodies on the MUSCAT assay and antigens to immunize rabbits to develop antibody-positive controls. Subsequently, this quality-certified serum autoantibody monitoring system also demonstrated successful immune monitoring using clinical samples. In a clinical trial, adenovirus−mediated REIC/Dkk−3 (Ad-REIC) gene therapy has shown a successful clinical response in metastatic castration-resistant prostate cancer [52-54]. Ad-REIC is known to induce cancer cell-specific apoptosis [55] and activate the antitumor immune response [56, 57], so this serum sample was used to evaluate the MUSCAT assay system in the current study. It was confirmed that the elevated autoantibody biomarker closely related to the clinical response showed potential to assist clinical decisions by monitoring the level of the cancer-immunity cycle.

Materials and Methods

Preparation of Recombinant Antigens

The cDNAs for antigens encoding the full-length and mature form of NY-ESO-1/CT6.1 (Uniprot: P78358), MAGE-A4/CT1.4 (Uniprot: P43358), XAGE-1b/CT12.1 (Uniprot: Q9HD64), MAGE-C2/CT10 (Uniprot: Q9UBF1), DDX53/CT-26 (Uniprot: Q86TM3), WT-1 (Uniprot: J3KNN9), CEP55 (Uniprot: Q53EZ4), LY6K/CT97 (Uniprot: Q17RY6), PSG8 (Uniprot: Q9UQ74), and ZNF165/CT53 (Uniprot: P49910) were cloned into pET28b vectors (Novagen) to express a His-tag (MGSSHHHHHHSSGLVPRGSH) on the N-terminus, and StrepTagII (GPGWSHPQFEK) on the carboxyl terminus. An expression vector for enhanced green fluorescent protein (EGFP) was designed using the same procedure. All recombinant proteins were expressed in Escherichia coli BL21(DE3). MAGE-A4, MAGE-C2, and EGFP expressed as soluble fractions were purified by immobilized metal affinity chromatography (IMAC). The other eight recombinant proteins expressed as insoluble inclusion bodies were solubilized by reversible S-cationization using [3-(trimethylammonium)propyl]-methanethiosulphonate (TAPS-sulfonate, Katayama Chemical, Osaka, Japan), as described previously [32, 35, 36]. Antigens, containing degraded impurities, were further purified by a reversed-phase HPLC column (COSMOSIL Protein-R, 4.6 mm I.D. × 150 mm, Nacalai Tesque Inc.) using an acetonitrile linear gradient elution procedure, in the presence of 0.1% HCl (Figure 1-2).

Immunization and Purification of Polyclonal Antibody

Antiserums against ten recombinant antigens were prepared by Cosmo Bio (Tokyo, Japan) by immunizing rabbits with native MAGE-A4 or nine TAPS-antigens. The IgG fraction was precipitated using 40% ammonium sulfate and dialyzed against PBS. The sample was then diluted three times with 60 mM acetate buffer (pH 4.8), and 6.8% caprylic acid was added to precipitate fibrinogen [58]. After dialysis against PBS, anti-HisTag and anti-StrepTagII antibodies were captured using HisTag-EGFP-StrepTagII protein-immobilized NHS-sepharose (GE Healthcare). Specific antibodies against each antigen were purified using each antigen-immobilized column from the pass-through fractions described above.

Cell Culture

Human lung cancer-derived cell lines (NCI-H1299, NCI-H1975, and A549), a cervical cancer-derived cell line (HeLa S3), and an ovarian cancer-derived cell line (SK-OV-3) were obtained from the American Type Culture Collection (Manassas, VA, USA). The cells were maintained at 37°C with 5% CO2. All cell lines were cultured in RPMI 1640 medium supplemented with 10% fetal bovine serum and penicillin/streptomycin (Wako, Osaka, Japan). DNA demethylation was demonstrated by the addition of 5 μM 5-aza-2'-deoxycytidine (decitabine, DAC, LC Laboratories, Woburn, MA, USA) to the cell culture [59].

Western Blot Analysis

Cultured tissue cells were lysed in lysis buffer supplemented with a protease inhibitor cocktail and disrupted on ice using a sonicator. The protein concentration of cell lysates was assessed using the Bradford protein assay (Bio-Rad Laboratories, Hercules, CA, USA) with bovine serum albumin as a standard. Each cell lysate (20 μg) was subjected to SDS-PAGE using a 5-20% gel (Wako, Osaka, Japan) and transferred to a PVDF membrane. After blocking with PVDF-blocking reagent (Toyobo, Osaka, Japan), 1 μg/mL of purified polyclonal antibody for each antigen in Can Get Signal 1 (Toyobo) were incubated with the membrane. Immunoreactive antigens were detected using anti-rabbit IgG HRP-linked antibody (Cell Signaling Technology, Tokyo, Japan) and Western Lightning Plus ECL (PerkinElmer, Waltham, MA, USA). The control monoclonal antibodies to MAGE-A4 (clone: E701U, Cell Signaling Technology, Tokyo, Japan) and XAGE-1b (clone: USO9-13) [60] were employed for the validation of the specificity of polyclonal antibodies. The membrane was reprobed with an anti-β-tubulin antibody (Wako).

Reverse Transcription (RT)-PCR

Total RNA was isolated from cultured tissue cells using the ISOSPIN Cell & Tissue RNA kit (Nippon Gene, Tokyo, Japan). First-strand cDNA was synthesized from 500 ng of total RNA using PrimeScript™ IV 1st strand cDNA Synthesis Mix (Takara Bio, Shiga, Japan). Gene expression of antigens was evaluated by PCR using primer pairs for NY-

ESO-1 (F: 5′- ACATACTGACTATCCGACTGAC-3′; R: 5′-AGGCTGAGCCAAAAACAC-3′), MAGE-A4 (F: 5′-AAACCAGCTATGTGAAAGTCC-3′; R: 5′-ACTCCCTCTTCCTCCTCTAAC-3′), and XAGE-1b (F: 5′-GAGCCCCAAAAAGAAGAACC-3′; R: 5′-GCTCTTGCAGATCACCTTCC-3′). Housekeeping gene expression was confirmed using the PCR primer pair for β-actin (F: 5′-AGAGCTACGAGCTGCCTGAC-3′; R: 5′-AGCACTGTGTTGGCGTACAG-3′).

Immunostaining of Endogenous CTAs

Sub-confluent cells on a glass-base dish (Iwaki Glass, Shizuoka, Japan) were fixed with 4% paraformaldehyde phosphate buffer solution (Wako) and permeabilized with 0.1% Triton X-100 in PBS for 30 min. Intracellular antigens were reacted with 5 μg/mL of purified polyclonal antibody for each antigen in PBS for 1 h at room temperature. Immunoreacted antigens and nuclei were stained with 2 μg/mL of goat anti-rabbit IgG, Alexa Fluor488 conjugated antibody (Life Technologies), and DAPI (Dojindo Laboratories, Kumamoto, Japan), respectively. Fluorescent images were acquired using a BC43 confocal microscope (Oxford Instruments, Abingdon, UK). Immunostaining of MAGE-C2 in tissue sections was performed using commercially available antibodies (HPA062230, Atlas Antibody, Stockholm, Sweden).

Validation of Luminex Beads and Beads Assay

Eight TAPS-antigens and two native antigens, certified for their purity, were immobilized to Bio-Plex Pro™ Magnetic COOH Beads (Bio-Rad) designed on a 10-plex assay panel (color-code:#27,35,37,43,45,46,53,55,62,64), according to the manufacturer's instructions. Beads assay for patient sera and titration assay by affinity-purified polyclonal antibodies designed as a positive control for the 10-plex assay were performed as described previously [32]. Briefly, serially diluted antisera in Block Ace (DS Pharma Biomedical, Osaka, Japan) were incubated with 1000 beads for each antigen-immobilized bead in a 96-well microplate (Greiner Bio-One, Tokyo, Japan). After washing with Bio-Plex Pro wash station (Bio-Rad), antibodies on beads were detected by biotin-conjugated, either anti-human IgG or anti-rabbit IgG (Vector Laboratories) and

labeled with streptavidin-PE (Vector Laboratories). Analysis was performed with Bio-Plex200 (Bio-Rad), and the mean fluorescence intensity (MFI) was determined from the values for 50 events (beads) per antigen at a minimum.

Immune Monitoring Study

A 63-year-old man with metastatic castration-resistant prostate cancer, who had shown promising results by Ad-REIC gene therapy, was chosen for the case study [52]. Frozen serum samples from a clinical trial on metastatic castration-resistant prostate cancer treated with Ad-REIC (UMIN-CTR ID: UMIN000004929) [52, 53] were used for antibody monitoring. The participants provided written informed consent under institutional review board permission at Okayama University Hospital. The prostate-specific antigen (PSA) level in serum was used from previous data. Control human serum from ten healthy donors (five male and five female, ages 19 to 64), and pooled serum from ten donors (five male and five female, ages 19 to 49) were obtained from Tennessee blood services (TN, USA).

Results

Characterization of Rabbit Antibody Immunized by Reversibly S-Cationized Antigen

Specific antibodies recognizing human CTAs or TAAs are useful as positive controls to validate quantitative antibody detection arrays. Most recombinant CTAs/TAAs are expressed as insoluble inclusion bodies in the E. coli expression system; S-cationization techniques allow for the preparation of water-soluble antigens. Several antigens required purification by reversed-phase HPLC because degraded products were also solubilized during the preparation of *S*-cationized protein (Figure 1-2). All recombinant antigens used in this study were verified by SDS-PAGE (Figure 1-3). In this study, the native conformation of MAGE-A4 as well as reversibly *S*-cationized TAPS-NY-ESO-1 and TAPS-XAGE-1b were used to confirm the availability of the antigens for immunization of rabbits (Figure 1-4).

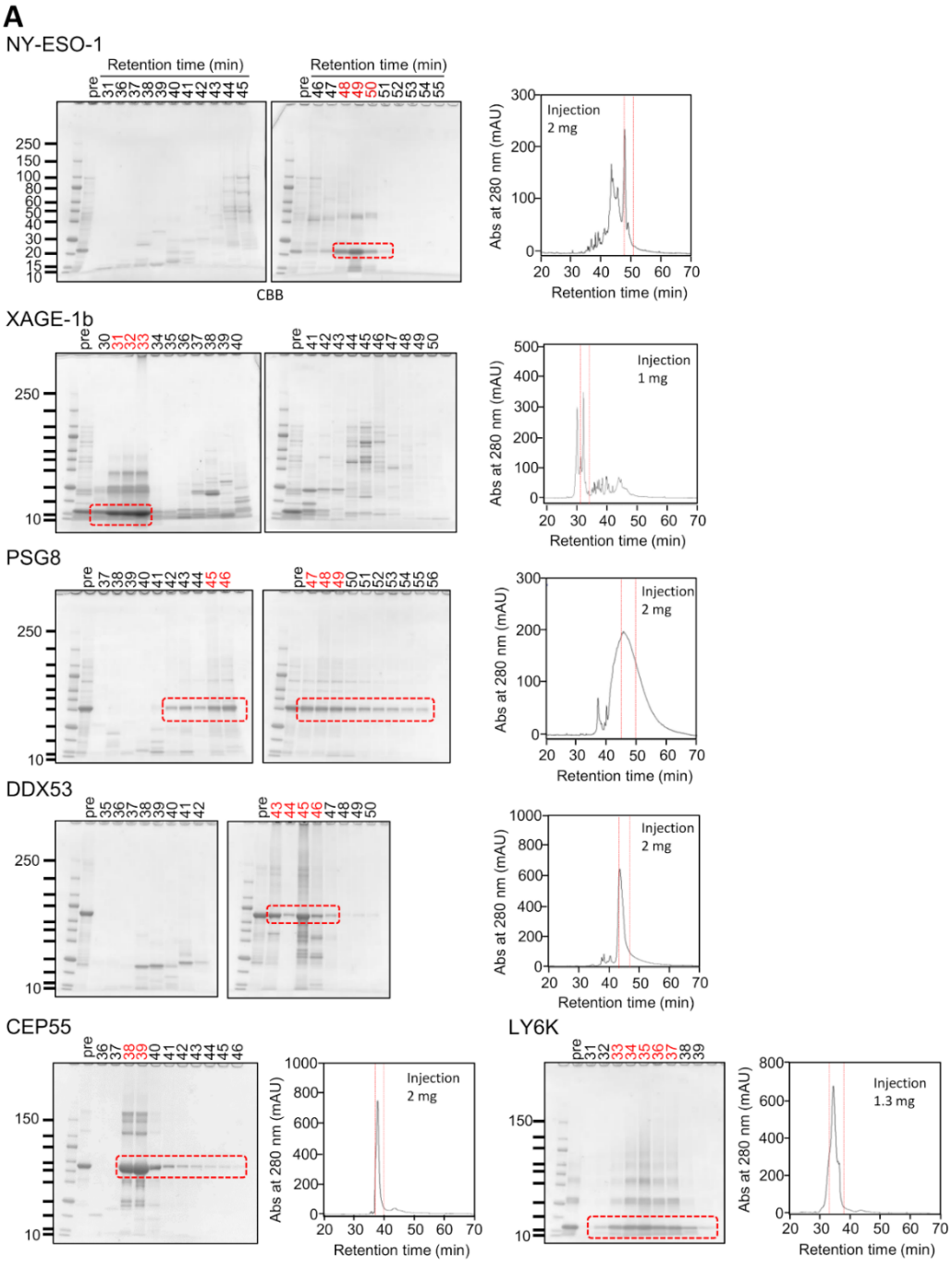
A
NY-ESO-1
Retention time (min)
Retention time (min)
pre 31 36 37 38 39 40 41 42 43 44 45
pre 46 47 48 49 50 51 52 53 54 55
250 150 100 80 60 50 40 30 20 15 10
CBB
Injection 2 mg
Abs at 280 nm (mAU)
Retention time (min)
XAGE-1b
pre 30 31 32 33 34 35 36 37 38 39 40
pre 41 42 43 44 45 46 47 48 49 50
250 10
Injection 1 mg
Abs at 280 nm (mAU)
Retention time (min)
PSG8
pre 37 38 39 40 41 42 43 44 45 46
pre 47 48 49 50 51 52 53 54 55 56
250 10
Injection 2 mg
Abs at 280 nm (mAU)
Retention time (min)
DDX53
pre 35 36 37 38 39 40 41 42
pre 43 44 45 46 47 48 49 50
250 10
Injection 2 mg
Abs at 280 nm (mAU)
Retention time (min)
CEP55
pre 36 37 38 39 40 41 42 43 44 45 46
150 10
Injection 2 mg
Abs at 280 nm (mAU)
Retention time (min)
LY6K
pre 31 32 33 34 35 36 37 38 39
150 10
Injection 1.3 mg
Abs at 280 nm (mAU)
Retention time (min)

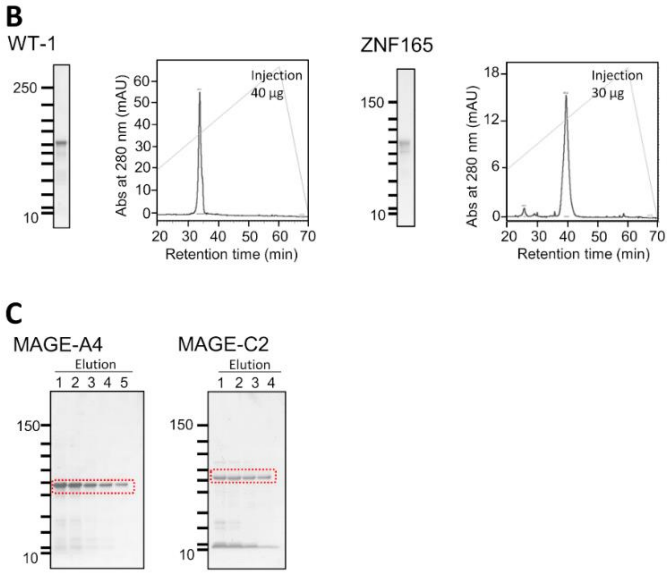

Figure 1-2 Preparation of recombinant antigens.

(A) Chromatographic pattern and SDS-PAGE results for six TAPS antigens. The red dotted boxes indicate the area containing the antigens. The fractions highlighted in red were pooled before immobilization on Bio-Plex Pro™ Magnetic COOH Beads . **(B)** Chromatographic pattern and SDS-PAGE results for TAPS-WT-1 and TAPS-ZNF165, both samples exhibited greater than 95% purity. **(C)** SDS-PAGE results for MAGE-A4 and MAGE-C2, both were purified by IMAC. The red dotted boxes indicate the area containing the antigens. Samples shown in (B) and (C) were immobilized to Bio-Plex Pro™ Magnetic COOH Beads without purification by a reversed-phase HPLC column.

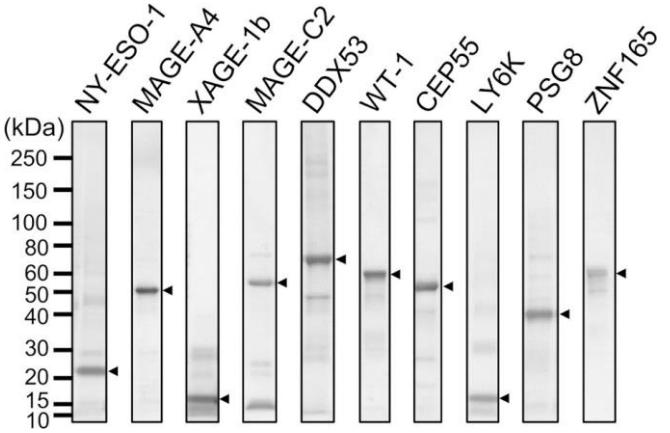

Figure 1-3 SDS-PAGE analysis of antigens employed for MUSCAT assay.

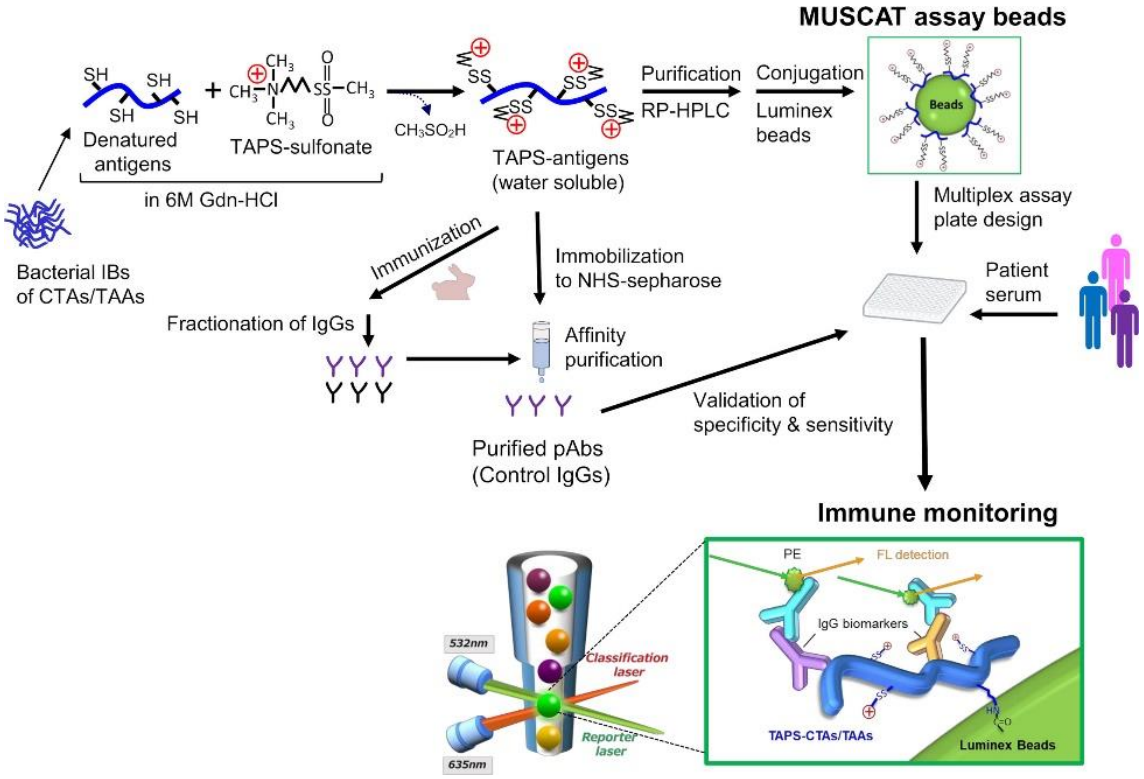

Figure 1-4 Schematic presentation of antigen engineering of CTAs/TAAs based on solubilization of denatured proteins by *S*-cationization techniques.
Water-soluble and full-length TAPS-antigens were employed to capture specific antibodies for immune monitoring and immunization antigens to develop the control IgGs.

These antisera showed high sensitivity to detect the endogenous level of intracellular antigens in western blotting and immunofluorescence staining (Figure 1-5A, B). Although both NY-ESO-1 and XAGE-1b were immunized as alkyldisulfide-modified forms, antibodies raised in rabbits specifically recognized linear epitopes in denatured antigen (Figure 1-5A), as well as epitopes in the native conformation (Figure 1-5B). The antigen specificity between purified polyclonal antibodies and monoclonal antibodies was almost comparable. Antibody response patterns for XAGE-1b are complicated because there are multiple variants (Figure 1-6). The nuclear localization of the granular-like pattern of XAGE-1b in NCI-H1975 cells was consistent with previous immunohistochemical results in lung cancer tissues and cells [19, 61]. This specific antibody is also detectable in the epigenetically regulated expression of CTAs. SK-OV-3 cells treated with DNA-methylation inhibitor of decitabine (DAC) showed induction of NY-ESO-1, MAGE-A4 and XAGE-1b as determined by measuring mRNA and protein expression levels (Figure 1-5C, D).

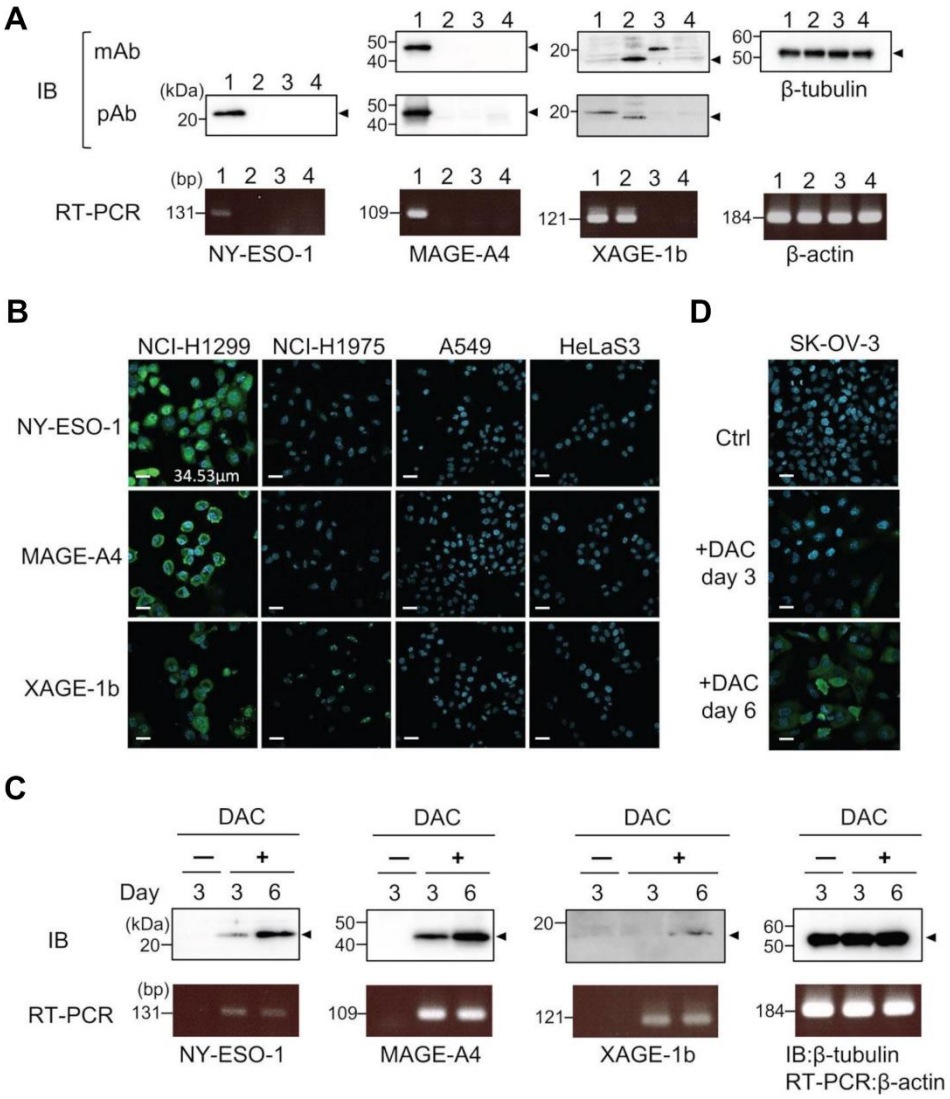

Figure 1-5 Specific binding of control IgGs developed by TAPS-antigen immunization was confirmed by the binding study of endogenous antigens.

(A) Detection of intracellular antigens in cell lysates lane 1, NCI-H1299; lane 2, NCI-H1975; lane 3, A549; lane 4, HeLa S3 cells. Cell lysates were analyzed by western blotting with monoclonal antibodies or polyclonal antibodies (upper). mRNA expression levels of each antigen were evaluated by RT-PCR (lower). **(B)** Immunofluorescence staining of NCI-H1299, NCI-H1975, A549, and HeLa S3 cells for nucleus (blue) and intracellular antigens (green). **(C)** Detection of induced CTAs expression protein in SK-OV-3 cells treated with 5 μM DAC. Samples were collected after three or six days of cultivation with DAC. The upper panel is western blotting, the lower panel is RT-PCR. **(D)** Immunofluorescence staining of SK-OV-3 cells treated with 5 μM DAC for nucleus (blue) and intracellular NY-ESO-1 (green).

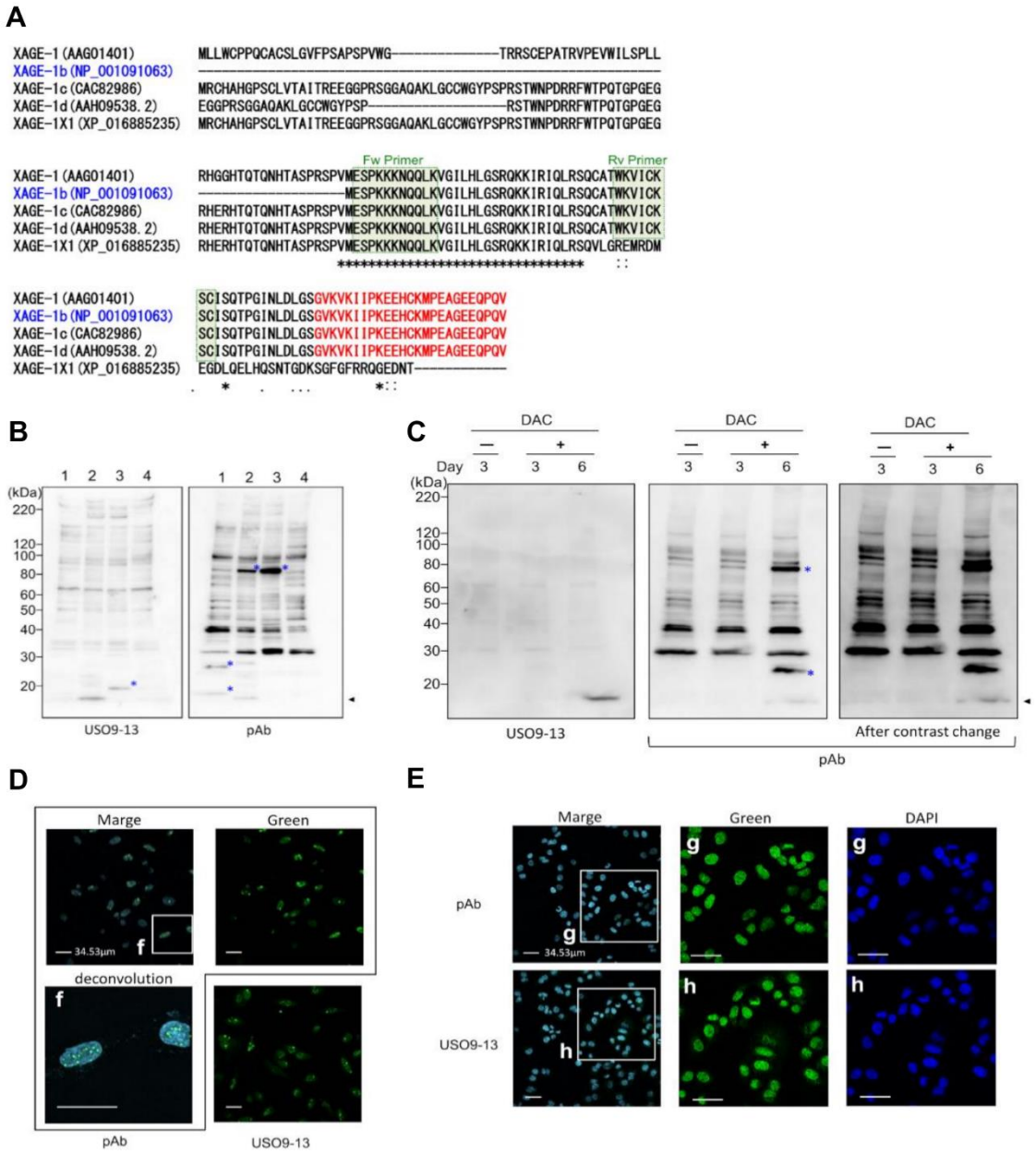

Figure 1-6　XAGE-1 variants and immune reactivity of endogenous protein.

(A) Protein sequence alignment of XAGE-1, XAGE-1b, XAGE-1c, XAGE-1d, and XAGE-1X1 indicating the primer binding sites for RT-PCR (green box). **(B)** Detection of endogenous antigens in cell lysates, lane 1, NCI-H1299; lane 2, NCI-H1975; lane 3, A549; lane 4, HeLa S3 cells. Cell lysates were analyzed by western blotting, using XAGE-1b monoclonal antibody (USO9-13) or polyclonal antibody (pAb). * indicates the presumed XAGE-1 variants. **(C)** Detection of induced XAGE-1b expression protein by western blotting, using authorized XAGE-1b monoclonal antibody (USO9-13) or polyclonal antibody (pAb), in cell lysates of SK-OV-3 treated with 5 μM DAC. Samples were collected after three or six days of incubation with DAC. * indicates the presumed XAGE-1 variants. **(D)** Immunofluorescence staining of NCI-H1975 cells for nucleus (blue) and intracellular XAGE-1b (green) showing. XAGE-1b predominantly localized to the nucleus with characteristic dotted distribution. **(E)** Immunofluorescence staining of A549 cells for nucleus (blue) and intracellular XAGE-1b (green) indicating XAGE-1 variants localized to both the cytoplasm and nucleus.

Validation of MUSCAT Assay Panel

The specific binding of purified rabbit polyclonal anti-CTA antibodies was confirmed using both single-plex and 10-plex bead assays (Figure 1-7 A). After purification of each specific antibody using an antigen-immobilized column, linearity and dynamic range of antibody detection in the MUSCAT assay were successfully confirmed in both single and 10-plex assays. The MFI values, calculated from more than 50 beads events in single and 10-plex assays, were highly correlated (Figure 1-7 B). The detection ranges for NY-ESO-1(0.32-231 ng/mL), MAGE-A4 (0.12-489 ng/mL), and XAGE-1b (0.08-50 ng/mL) indicated the high sensitivity of these specific antibodies. Although every antigen was designed to possess HisTag and StrepTagII, no cross-reactivity was observed with the purified antibodies. Using this procedure, the preparation of all sets of specific antibodies will be an excellent tool for certifying the specificity and sensitivity of the MUSCAT assay inter-assay or preparation lot.

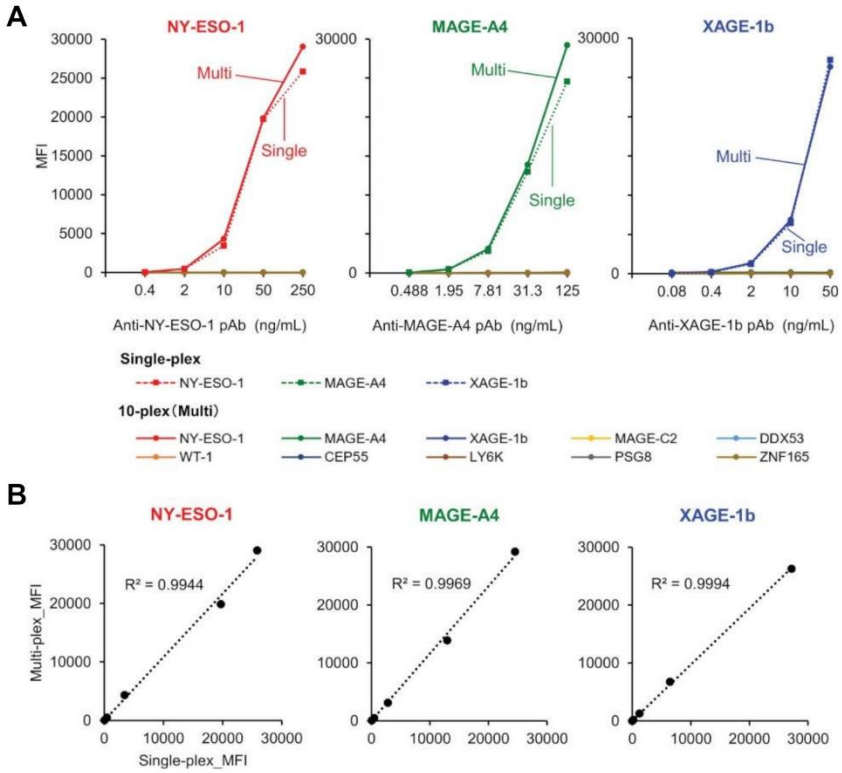

Figure 1-7 The validation study used purified rabbit polyclonal anti-CTAs antibodies in the single-plex and 10-plex beads assay.
(A) The solid line represents the 10-plex assay, and the dotted line indicates the single-plex assay.
(B) Correlation analysis between single-plex and 10-plex assay.

Monitoring of Activation of Cancer-Immunity Cycle by Autoantibodies

To evaluate the potency of the MUSCAT assay system, changes in serum autoantibody levels were evaluated in one patient successfully treated with Ad-REIC cancer gene therapy [52]. Intratumoral injection of Ad-REIC into metastatic lymph nodes induces ER stress-mediated apoptosis by overexpression of REIC, which is then extracellularly secreted where it upregulates immune reactions. Thus, tumor regression is thought to be related to activation of the cancer-immunity cycle. As shown in Figure 1-8A, drastic upregulation of anti-MAGE-C2 and anti-DDX53 was observed during the therapy. Other antibodies for WT-1, ZNF165, MAGE-A4, and PSG8 also increased along with the therapy, typically representing antigen spreading. One of the drastically induced anti-MAGE-C2 antibodies was confirmed to induce immune responses in tumor microenvironments because MAGE-C2 was detected in pretreatment biopsy (Figure 1-8B).

This clinical trial succeeded in complete regression of metastatic castration-resistant prostate cancer by repeating 17 intratumoral injections of Ad-REIC for more than two years [52]. Notably, the earlier detection (approximately day 170) of increased autoantibody level before the PSA level decreasing is an important aspect of clinical use of the MUSCAT assay. In addition to the remission of cancer by Ad-REIC, autoantibodies were also reduced. The disappearance of antigen stimulation seems to be closely related to antibody levels. The detection of moderate activation of the cancer-immunity cycle by a small aliquot of a blood sample will be an excellent value for the decision of treatment course.

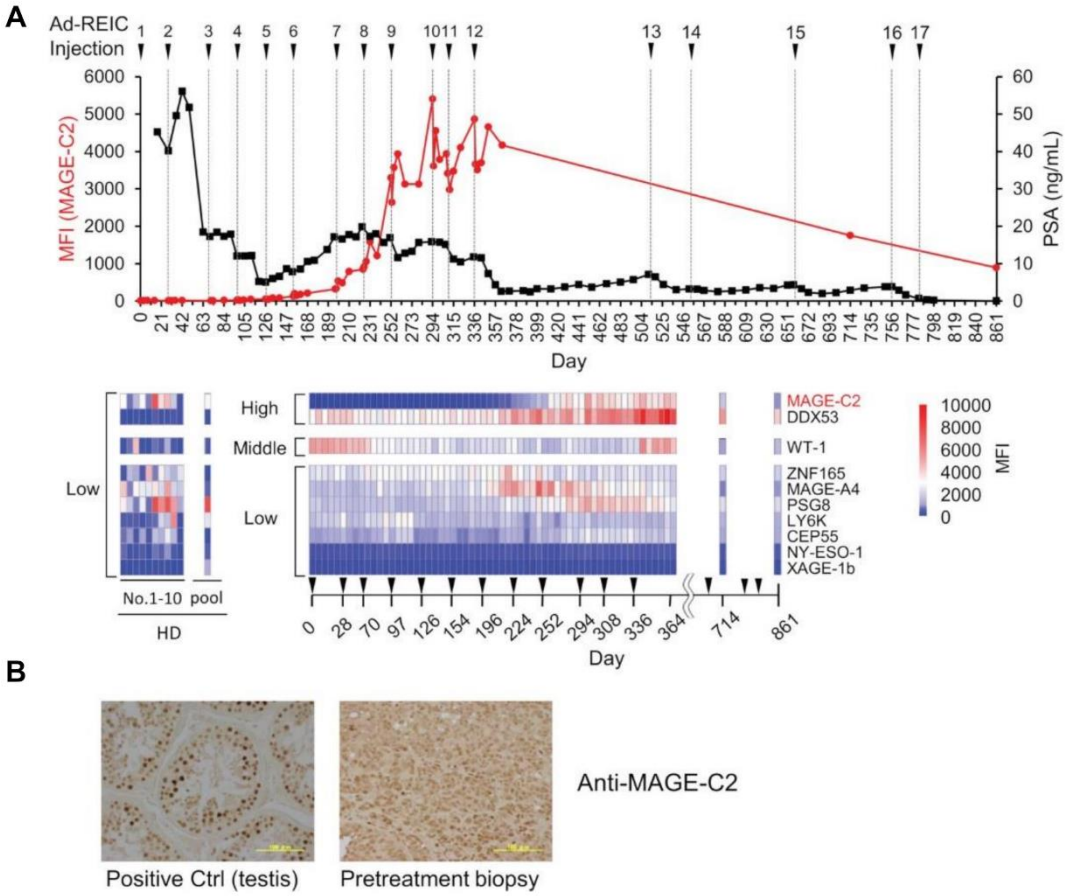

Figure 1-8 Demonstration of immune monitoring by MUSCAT assay panel on a single, patient-derived clinical sample.

(A) The line graph represents anti-MAGE-C2 antibodies and PSA changes. The heat map shows changes in the levels of 10 different serum autoantibodies. The dilution ratio of serum autoantibodies was adjusted to 80,000-fold dilution for high titer, 16,000-fold dilution for middle antibody titer, and 1,600-fold for low titer samples. Autoantibody levels in ten healthy donor individuals and a pooled sample. **(B)** Detection of MAGE-C2 protein in the tumor tissues. Scale bar represents 100 μm.

Discussion

A recent oncological study revealed that cancer is heterogeneous [7]. Heterogeneity in cancer is not only limited to different patients but also occurs within a single patient [8]. Certain tumors can be analyzed by molecular profiling yielding clinically relevant diagnostic and prognostic results [7]. However, intrapatient or intratumoral heterogeneity remains a significant challenge for deciding the course of clinical cancer treatment. As such, activating the cancer-immunity cycle is a reasonable strategy to overcome this heterogeneity issue [7]. The death of the heterogeneous population of cancer cells can be a trigger for priming naïve T cells by newly exposed antigens, resulting in the activation

of the cancer-immunity cycle. Antigen exposure from cancer cells also enhances pre-existing memory T and B cells. Upon induction of these immune responses, T cell-mediated cellular immunity targeting various tumor antigens may help regress heterogeneous cancer. Humoral immune responses also increase during the cancer-immunity cycle activation (Figure 1-1); therefore, anti-CTA/TAA IgGs are biomarkers that can reflect this anticancer immunity. The IgG autoantibody biomarker is superior in physicochemical aspects because IgGs in peripheral blood are relatively stable proteins [62]. Furthermore, the bias in sampling or storage conditions are nearly negligible.

The preparation of a comprehensive array set of CTAs/TAAs is preferable for reliable evaluation of antigen spreading. Each antigen-specific antibody assay must be validated for its specificity and sensitivity for clinical use. In this study, the water-soluble full-length reversibly *S*-cationized TAPS-antigen was demonstrated to employ both antigens to capture specific antibodies in assay and antigens to develop the antibody in the immunized animals. Purified antibodies reliably validated control in the MUSCAT assay system. Most CTAs have unstable and aggregation-favored properties [29]; therefore, S-cationization is a powerful technique to prepare highly purified and water-soluble antigens. We are currently preparing comprehensive sets of CTAs/TAAs and each specific antibody for use as a validation tool using these procedures.

The preparation of CTA-specific antibodies also allowed us to gain an understanding of the structural properties of the CTAs (Figure 1-5). TAPS-CTAs are fully denatured, so antibodies immunized by them recognize linear epitopes. However, these antibodies also recognize intracellular endogenous CTAs under non-denaturing conditions. This strongly suggests that the conformation of CTAs has no rigid conformation in cells. CTAs are originally found in testicular cells and are predicted to form a cooperative structure [30]. However, aberrantly expressed CTAs in cancer lack this cooperative expression. Therefore, the CTAs released from apoptotic cancer cells are supposed to be easy to denature or decompose. Antibody-producing cells proliferate that bind to cancer antigens released from dead cancer cells; thus, most anti-CTAs bind to the denatured form of protein. A class switch from IgM to IgG also requires antigen binding and cytokine stimulation [63]. This mechanism explains why anti-CTAs are recognized preferably in linear epitopes (Figure 1-1).

Many CTAs, including MAGE-A4, NY-ESO-1, and XAGE-1b, are located on the X chromosome and are epigenetically regulated. Lack of X chromosome inactivation in cancer cells induces aberrant epigenetic changes and CTAs expression. Highly immunogenic cancer cells, expressing CTAs, tend to be targeted by the host immune system; thus, suppression of CTAs by DNA methylation could be a mechanism of immune escape in cancer [64, 65]. DNA methylation inhibitor treatment, to upregulate the immunogenicity of tumors, would therefore facilitate targeting by the host immune system [66]. Ovarian cancer cell line SK-OV-3, has been reported as a model for reactivation of NY-ESO-1 by DAC [67]. Increased levels of CTAs after DAC treatment were detected using anti-CTAs antibodies (Figure 1-5C, D). The polyclonal antibodies, immunized full-length CTAs, detected endogenous antigens and their transcript variants. Interestingly, XAGE-1b includes various uncharacterized immune reactive variants (Figure 1-6). Determination of these target antigens is crucial for enhancing the accuracy of the immune monitoring system.

As discussed above, both antigen exposure by inducing apoptosis in cancer cells and releasing immune-suppressing machinery is critical to upregulate the cancer-immunity cycle. Intratumoral injections of Ad-REIC therapy are potent in inducing both effects [52]. In this therapy, Ad-REIC was injected into the metastatic lymph nodes. This strategy may contribute to the upregulation of the cancer immunity cycle because the released antigens from apoptotic cells exist in lymph nodes and stimulate T and B cells efficiently (Figure 1-1 and Figure 1-8). Although the validation of the MUSCAT assay has not yet been completed by positive control of antibodies, this panel showed successful immune monitoring by detecting upregulation of several antibodies in the high responders by Ad-REIC cancer gene therapy. It is crucial for the diagnostic use of the MUSCAT assay that antigen spreading be observed before tumor regression. Baseline analysis of these autoantibodies showed individual variations in ten healthy donors (Figure 1-8A) although it is unclear whether these variations reflect the immune history of the individuals. However, monitoring autoantibody changes during therapy will evaluate the generation of cancer-immunity cycle and autoimmune responses. The concept of immunologically “hot” or “cold” from the outcome of immune checkpoint inhibitor therapy is widely accepted today, and the drug discovery to achieve “cold-to-hot” tumor conversion is a

great challenge [46]. Thus, a tool to monitor this conversion is critical. A highly accurate and quantitative autoantibody monitoring system will be an excellent tool for developing a therapeutic strategy to overcome refractory cancer.

Chapter2 Validation study of MUSCAT-assay system

Abstract

Autoantibodies against tumor-associated antigens (TAAs) or cancer/testis antigens (CTAs) detect in cancer patients due to the long-term interaction between the immune system and cancers. Thus, these antibodies are potent to be used as biomarkers reflecting the level of anti-tumor immune responses or prediction of immune therapy efficacy. The validation of the autoantibody assay system is critical for the accurate biomarker study. To quantitatively assess comprehensive anti-TAAs/CTAs antibodies, we report the validation study for the multiple S-cationized antigen-immobilized bead array (MUSCAT)-assay systems. The quality of antigen-immobilized beads was successfully verified by the dynamic range, linearity, intra-assay, and inter-assay accuracy using a positive control antibody developed in immunized rabbits. We also confirmed the high quality of the intra-assay coefficient of variations (CV%) to be less than 20% and the inter-assay CV% to be less than 30%. The assay panel also validated intra- and inter-assay accuracy using plasma from 120 healthy donors. Comparing autoantibody profiles from 162 non-small cell lung cancer (NSCLC) patients showed higher autoantibody levels than healthy donors. This result strongly suggests that autoantibodies reflect anti-tumor immune responses in NSCLC patients. However, autoantibodies are also detectable in healthy donors; thus, analysis of immune responses should account for the baseline level of autoantibodies. This study establishes a guaranteed range of measurement accuracy in evaluating autoantibodies in the MUSCAT-assay system clinical specimens. Because autoantibodies are stable and quantitatively detectable from small aliquots of peripheral blood, immune profiling or monitoring by this panel will contribute the accurate, personalized precision medicine regarding immune-related disorders.

Introduction

Immune checkpoint inhibitors (ICIs) have shown superior clinical efficacy over conventional cancer treatments such as surgery, chemotherapy, and radiation therapy. However, their clinical responses vary from patient to patient due to the complexity of tumor-immune interactions. Clinical benefits with anti-PD-1/PD-L1 monotherapy are only 20–30% overall response rate in non-small cell lung cancer (NSCLC) [68]. Inhibition of immune checkpoint benefits the upregulation of antitumor immune responses, and the risk of immune-related adverse effects (irAE) increases as a disadvantage [69]. Thus, the diagnostic tool demanded to predict who will respond to cancer immunotherapies and who has the risk of irAE before beginning ICI therapy. Because the tumor microenvironment (TME) reflects well of immune status, direct evaluation using tumor biopsy is now available in clinical sites.

The level of PD-L1 protein expression in tumor tissues is suggested to relate to immunity hot TME. A tumor proportion score (TPS) of more than 50%, a scoring percentage of membrane immune staining of anti-PD-L1, is used to predict responder patients by pembrolizumab (anti-PD-1) monotherapy on advanced NSCLC [70]. The somatic gene mutation-derived proteins in the cancer cells, referred to as neoantigen, is a potential target of immune cells. Tumor mutation burden (TMB) determined by cancer cell exosome analysis is used to predict tumor immunogenicity [71, 72]. Likewise, high microsatellite instability (MSI-H) caused by mismatch repair deficiency (dMMR), which is known to relate to colorectal cancer, also reflects higher contents of neoantigens. TMB and MSI-H scores are employed to estimate tumor immunogenicity. Tumor infiltration of immune cells and cancer-associated fibroblast in TME are also critical for antitumor immunity. RNA-sequencing of tumor biopsy can evaluate the cellular component in TEM and emerge as an excellent tool for classifying tumor immune status [73].

As described above, to know the TME for precision cancer immune therapy, tumor tissue biopsy methods are currently employed in diagnosis. However, there are several limitations because of invasiveness to patients or heterogeneity of tumors, especially when repeated diagnosis and monitoring are required [74]. Alternative, less invasive circulating biomarkers reflecting the TME and tumor immune status are demanded in cancer precision immune therapy.

Autoantibody biomarkers against cancer antigens, such as TAAs or CTAs, are mechanistically linked to the antitumor immune responses [20, 24-27]. Tumor cells are known to express several kinds of abnormal proteins not expressed in normal cells. After immune responses lysed cancer cells, some abnormal proteins work as cancer antigens. Immune cells recognize these antigens, producing autoantibodies as humoral immune responses. Therefore, the existence of autoantibodies, means of profiling, reflects the tumor immunogenicity in vivo, and the level of autoantibodies, means of monitoring, reflect the antigen stimulation to the B-cells. The former of autoantibody profiling requires comprehensiveness of antigen array because of individual variation. The latter of autoantibody monitoring has to validate the accuracy of the assay system.

According to the above requirements, conventional enzyme-linked immunosorbent assay (ELISA) approaches are reliable in assay accuracy but need more comprehensiveness of antigens. The protein microarray assay can display comprehensive antigens, but it is challenging to verify each protein's quality and assay accuracy on a clinically appropriate level. Multiplex beads assay using the Luminex system, which can distinguish each antigen by fluorescent-coded magnetic beads, facilitate the design of ten to several hundred antigen arrays with higher accurate assay by flowcytometric statistical

analysis. This Luminex beads array system must use at suspension after conjugating purified antigens onto the fluorescent-coded magnetic bead. Autoantibodies in cancer patients are known to be polyclonal and recognize various epitopes [33]. Thus, recombinant antigens prefer to prepare as full-length antigens. One technical limitation is that most recombinant full-length TAAs/CTAs showed unstable and easy-to-aggregate properties [29, 33]. To overcome these issues, we use the Cys-specific chemical modification to endow cationic charge and prepare the water-soluble full-length antigens in denatured form. Combining the Luminex beads array system and *S*-cationized antigen preparation techniques, we developed the multiple *S*-cationized antigen-immobilized bead array (MUSCAT)-assay, a comprehensive and quantitative anti-cancer antigen-antibody detection system.

Clinical analysis of autoantibody biomarkers for precision cancer immune therapy requires a validated MUSCAT-assay system. Chapter 1 describes the methodology to prepare the control antibody for the validation of the MUSCAT-assay system, and this chapter 2 describes demonstrated beads validation in dynamic range, linearity, intra-assay, and inter-assay using 59 control antibodies. This assay panel was also validated and analyzed by serum from 120 healthy donors and 162 NSCLC patients. Although the methods for data analysis requires deep static analysis, autoantibody profile from 120 healthy donors will be reference data for analyzing the physiological significance of autoantibodies.

Materials and methods

Preparation of Recombinant Antigens

Recombinant antigens and their expression vectors and purification procedures are described in Table 2-1. Plasmid DNA cloning of each antigen into pET28 vector (Novagen) or CMV-TSC vector [75], IMAC purification from the soluble fraction, and S-cationization procedures from the insoluble fraction were described above[32, 35, 36, 76].

Table 2-1 Antigen information, vectors, and purification methods for the 119 recombinant antigens.

No.	Antigen information				Vector	No.	Antigen information				Vector
	Name	CT No	Uniprot	Expression			Name	CT No	Uniprot	Expression	
1	A1AT_Native	—	P01009-1	S	CMV	61	RalA_SCT	—	P11233	I	pET
2	A1AT_SCT	—	P01009-1	I	pET	62	RhoGDI_Native	—	P52565-1	S	pET
3	A2B1_Native	—	P22626-1	S	pET	63	RhoGDI_SCT	—	P52565-1	I	pET
4	A2B1_SCT	—	P22626-1	I	pET	64	SOX2_SCT	—	P48431	I	pET
5	AARS_SCT	—	P49588-1	I	pET	65	Survivin2b_SCT	—	O15392-2	I	pET
6	EEF1A1_SCT	—	P68104	I	pET	66	TCP1_SCT	—	P17987	I	pET
7	EEF1G_SCT	—	P26641	I	pET	67	WT-1_SCT	—	P19544-7	I	pET
8	EEF2K_SCT	—	O00418	I	pET	68	ACRBP_SCT	23	Q8NEB7	I	pET
9	FKBP4_Native	—	Q02790	S	pET	69	ACTL8_SCT	57	Q9H568	I	pET
10	HARS_SCT	—	P12081-1	I	pET	70	BAGE_SCT	2.3	Q86Y29	I	pET
11	HNRNPR_Native	—	O43390	S	pET	71	BORIS_SCT	27	Q8NI51-1	I	CMV
12	HNRNPR_SCT	—	O43390	S	pET	72	CABYR_Native	88	O75952-1	S	pET
13	KRT18_Intact	—	P05783	I	pET	73	CCDC36_SCT	74	Q8IYA8-1	I	pET
14	KRT8_Intact	—	P05787-1	I	pET	74	CCDC62_SCT	109	Q6P9F0-1	I	pET
15	LMNA_SCT	—	P02545	I	pET	75	CEP55_SCT	111	Q53EZ4-1	I	pET
16	PCNA_SCT	—	P12004	I	pET	76	CSAG2_SCT	24.2	Q9Y5P2-1	I	pET
17	PRDX2_Native	—	P32119-1	S	pET	77	CT156_SCT	156	Q8NHS0	I	pET
18	PRDX2_SCT	—	P32119-1	I	pET	78	CT45A1_SCT	45-1	Q5HYN5	I	pET
19	RO52_SCT	—	P19474-1	I	pET	79	Cxorf61_SCT	83	Q5H943	I	pET
20	RO60_SCT	—	P10155-1	I	pET	80	DCAF12_SCT	102	Q5T6F0	I	pET
21	RPL7A_SCT	—	P62424	I	pET	81	DDX53_SCT	26	Q86TM3	I	pET
22	TKT_SCT	—	P29401	I	pET	82	DPPA2_SCT	100	Q7Z7J5	I	pET
23	TPI1_Native	—	P60174-1	S	pET	83	FTHL17_SCT	38	Q9BXU8	I	pET
24	TPI1_SCT	—	P60174-1	I	pET	84	HORMAD1_Native	46	Q86X24-1	S	pET
25	Vim_SCT	—	P08670	I	pET	85	HORMAD1_SCT	46	Q86X24-1	I	pET
26	Wdr36_SCT	—	Q8NI36	I	CMV	86	HSPB9_SCT	51	Q9BQS6	I	pET
27	AFP_Native	—	P02771	S	CMV	87	LUZP4_SCT	28	Q9P127-1	I	pET
28	AFP_SCT	—	P02771	S	CMV	88	LY6K_SCT	97	Q17RY6-1	I	pET
29	CA125_Native	—	Q8WXI7	S	CMV	89	MAEL_SCT	128	Q96JY0-1	I	pET
30	CA125_SCT	—	Q8WXI7	S	CMV	90	MAGE-A1_SCT	1.1	P43355	I	pET
31	CA19-9_Native	—	Q969X2-1	S	CMV	91	MAGE-A4_Native	1.4	P43358	S	pET
32	CA19-9_SCT	—	Q969X2-1	I	pET	92	MAGE-A6_Native	1.6	P43360	S	pET
33	CEA_Native	—	P06731-1	S	CMV	93	MAGE-B3_SCT	3.3	O15480	I	pET
34	CEA_SCT	—	P06731-1	S	CMV	94	MAGE-A3_Native	1.3	P43357	S	pET
35	CYFRA_SCT	—	P08727	I	pET	95	MAGE-C1_Native	7.1	O60732-2	S	pET
36	SCC_Native	—	P29508-1	S	CMV	96	MAGE-C2_Native	10	Q9UBF1	S	pET
37	ALK.cd_SCT	—	Q9UM73	I	pET	97	MORC1_SCT	33	Q86VD1-1	I	CMV
38	ANXA1_Native	—	P04083	S	pET	98	NUF2_SCT	106	Q9BZD4	I	pET
39	ANXA1_SCT	—	P04083	I	pET	99	NXF2_SCT	39	Q9GZY0	I	pET
40	CCNB1_SCT	—	P14635-1	I	pET	100	NY-ESO-1_SCT	6.1	O75638-1	I	pET
41	CEACAM19_Native	CEACAM19	Q7Z692-1	S	CMV	101	OIP5_SCT	86	O43482	I	pET
42	CEACAM19_SCT	CEACAM19	Q7Z692-1	I	pET	102	PAGE5_Native	16.1	Q96GU1-1	S	pET
43	CEACAM4_SCT	CEACAM4	O75871	I	pET	103	PBK_SCT	84	Q96KB5-1	I	pET
44	EMD_SCT	—	P50402	I	pET	104	PLAC1_SCT	92	Q9HBJ0	I	pET
45	ENO1_SCT	—	P06733-1	I	pET	105	SEMG1_Native	103	P04279-1	S	CMV
46	EZR_Native	—	P15311	S	pET	106	SEMG1_SCT	103	P04279-1	I	pET
47	EZR_SCT	—	P15311	I	pET	107	SPA17_Native	22	Q15506	S	pET
48	gp100_SCT	—	P40967-1	I	pET	108	SPNAXD_SCT	11.4	Q9BXN6	I	CMV
49	Her2-ECD_Native	—	P04626-1	S	CMV	109	SPEF2(2)_SCT	122	Q9C093-4	I	CMV
50	HSP105_SCT	—	Q92598-1	I	pET	110	SSX2_SCT	5.2	Q16385-1	I	pET
51	MSLN_Native	—	Q13421-4	S	CMV	111	SSX4_SCT	5.4	O60224-1	I	pET
52	NPM1_Native	—	P06748-1	S	pET	112	SYCE1_SCT	76	Q8N0S2-2	I	pET
53	NPM1_SCT	—	P06748-1	I	pET	113	SYCP1_SCT	8	Q15431	I	CMV
54	p53_SCT	—	P04637-1	I	pET	114	TEKT5_SCT	149	Q96M29	I	pET
55	PDZD11_Native	—	Q5EBL8	S	pET	115	TFDP3_SCT	30	Q5H9I0	I	CMV
56	PPIB_Native	—	P23284	S	pET	116	TSSK6_SCT	72	Q9BXA6	I	pET
57	PPP1CA_SCT	—	P62136-1	I	pET	117	XAGE-1b_SCT	12.1	Q9HD64-2	I	pET
58	PSG5_SCT	—	Q15238	I	pET	118	XAGE2_Native	12.2	Q96GT9	S	pET
59	PSG8_Native	—	Q9UQ74	S	CMV	119	ZNF165_SCT	53	P49910	I	pET
60	PSG8_SCT	—	Q9UQ74	I	pET						

Antigen names noted with _Native were purified proteins by IMAC-purification from the soluble fraction of cell lysates or secreted proteins in the medium. Antigens named with _SCT were solubilized antigens by *S*-cationization techniques from insoluble fraction followed by purified by reversed-phase HPLC, described in chapter 1. Antigens names with _Intact refolded from insoluble fraction without any chemical modifications.

Immunization and Purification of Polyclonal Antibody

Immunization and purification of polyclonal antibody were performed using previously reported methods [76].

Clinical samples

The human NSCLC patient's serum sample was obtained from Okayama University Hospital Biobank (Okadai Biobank, Japan), under the collaboration of Dr. Kiura K. and Dr. Ohashi　K. (Okayama University Hospital) of biomarker screening, approved by the ethics committee of Okayama University (Table 2-2).

Control human serum from 120 healthy donors (20 women and 20 men in their 20-39, 40-59, and 60-79 age groups, respectively) with no history of cancer or autoimmune diseases were obtained from the Tohoku Medical Megabank Organization (Japan).

Table 2-2　Summary of NSCLC patients' characteristic

patients	**n=162**
Age, years (range)	66.7 (37-83)
Sex, male / female	110 / 52
Histology, adeno / squamous / others/ unknown	108 / 41 / 11/ 2
Stage, III / IV / recurrence/ unknown	30 / 91 / 39/ 2

Luminex Beads and Beads Assay

120 antigens, certified for their purity, were immobilized to Bio-Plex Pro™ Magnetic COOH Beads (Bio-Rad) designed on assay panel (color-code:#26, 27, 35, 36, 37, 43, 44 45, 46, 52, 53, 54, 55, 62, 63, 64), according to the manufacturer's instructions. Beads assay for patient sera and titration assay by affinity-purified polyclonal antibodies designed as a positive control for the 10-plex assay were performed as described previously [32] . Briefly, serially diluted antisera in Block Ace (DS Pharma Biomedical, Osaka, Japan) were incubated with 1000 beads for each antigen-immobilized bead in a 96-well microplate (Greiner Bio-One, Tokyo, Japan). After washing with Bio-Plex Pro wash station (Bio-Rad), antibodies on beads were detected by biotin-conjugated, either anti-human IgG or anti-rabbit IgG (Vector Laboratories) and labeled with streptavidin-PE (Vector Laboratories). Analysis was performed with Bio-Plex200 (Bio-Rad), and the mean fluorescence intensity (MFI) was determined from the values for 50 events (beads) per antigen at a minimum.

Antigen immobilized beads validation by rabbit polyclonal antibodies

The quality of the antigen-immobilized beads was verified by 59 purified rabbit polyclonal antibodies. Seven-point dilution samples were prepared by making 2-fold or 4-fold serial dilutions of 59 purified rabbit polyclonal antibodies.

Dynamic range

Dynamic range (assay working range) is the range between the lowest level of quantification (LLOQ) and upper level of quantification (ULOQ) in which an assay is both precise and accurate. The LLOQ and ULOQ were calculated by analysis software (Bio-Plex Manager Softwere 6.2, Bio-Rad).

Linearity

Linearity was evaluated only for antibody concentration points that were within the dynamic range. The concentration was calculated from the titration curve. The slope and intercept were estimated using linear regression and the goodness of fit assessed using the linear correlation coefficient (R^2).

Precision

Precision was evaluated only for antibody concentration points that were within the dynamic range. Intra-assay %CV assessed variation among the replicates within the assay. Intra-assay %CV was calculated from the average of the %CV calculated from the MFI of all three replicates at each positive control antibody dilution point of two independent assays. Inter-assay %CV measured the variability across two independent assays. Coefficients of variation (CVs) were estimated using standard analysis of variance methods.

Assay validation by human healthy donor samples

Assay precision for 119 antigen-immobilized beads was evaluated in human-derived plasma from 120 healthy donors with a non-neoplastic, non-autoimmune clinical history. Intra-assay %CV assessed variation among the replicates within the assay. Intra-assay %CV was calculated from the MFI of all two replicates at each serum dilution point. Inter-assay %CV measured the variability across two independent assays.
Coefficients of variation (CVs) were estimated using standard analysis of variance methods.

Antigen batch and Antigen-immobilized bead batch reproducibility

The antigen and antigen-immobilized bead are the most critical reagent in the autoantibody assay. Therefore, it is essential to demonstrate batch to batch reproducibility. In this study, the reproducibility of antigen and antigen-immobilized bead batch was evaluated, with p53 protein as a representative. The evaluation by MUSCAT-assay was performed in the same method as the intra-assay for beads validation.

Antigen batch reproducibility

The reproducibility of the three batches of purified *S*-cationized p53 was evaluated by reversed-phase HPLC and MUSCAT-assay. Reversed-phase HPLC was used to evaluate the reproducibility of antigen purification of the antigen in the three lots. MUSCAT-assay was used to check the reproducibility of the signal intensity for the other three batches of antigen bound at the same time.

Antigen-immobilized bead batch reproducibility

The reproducibility of MUSCAT-assay signals was evaluated by using p53 immobilized beads prepared by the same antigens conjugated at different days.

Comparison of autoantibody distribution between NSCLC and healthy donor

The autoantibody profile in 120 healthy donors (HD) and 162 non-small cell lung cancer (NSCLC) patients was compared using results measured by MUSCAT-assay. The dilution ratio of serum was 200-fold dilution.

Results

Antigen immobilized beads validation by rabbit polyclonal antibodies

59 types of antigen-specific purified rabbit polyclonal antibodies verified the quality of antigen-immobilized Luminex beads. Specific binding of the control antibodies to the beads were assessed by the BioPlex system according to the procedures authorized to MUSCAT-assay for human-derived samples, except for the use of a secondary antibody of phycoerythrin-conjugated anti-rabbit IgG monoclonal antibody. The titration curve toward each antigen showed an antibody binding affinity-dependent manner (Figure 2-1). The positive control antibodies recognize multiple epitopes because of immunization of full-length antigens. This polyclonality is also similar to autoantibodies in human peripheral blood.

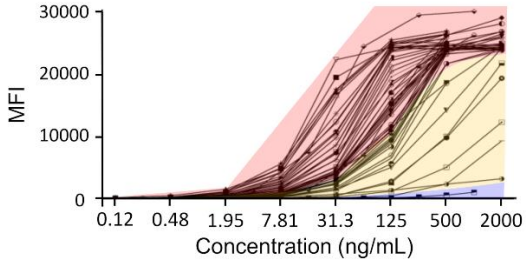

Figure 2-1 Titration profiles toward each antigen.

Overlaid titration profiles of 59 antigens obtained by measuring serial dilutions of rabbit polyclonal antibodies using MUSCAT-assay. The red box indicates high-affinity antibodies, the yellow box indicates medium- affinity antibodies, and the blue box indicates low-affinity antibodies.

Dynamic ranges of each antibody assay, between LLOQ and ULOQ, confirmed to show from ng/mL to sub-μg/mL level (Table 2-3A). This dynamic range corresponds to 10^{-11} M (1.5 ng/mL) to 10^{-9} M (150 ng/mL) of IgG. The standard procedure for the MUSCAT-assay uses 1/200 diluted serum or plasma; thus, the 5×10^{-9} to 5×10^{-6} M of IgGs in peripheral blood is the actual range of this assay. These dynamic ranges are reasonable to cover effective antibody concentrations because most antibodies are estimated to have K_D values in the low micromolar (10^{-6}) to nanomolar (10^{-7} to 10^{-9}) range.

The linearity of the antibody titers assessed by the MUSCAT-assay system was confirmed using dilution points (4~6 points) within the dynamic range of each positive control IgGs. As shown in Figure 2-2, all titration can fit the slope close to 1.0 and the intercept close to zero. Correlation coefficients were more than 0.998, thereby demonstrating satisfactory goodness of fit.

The precision of the MUSCAT-assay system was evaluated by intra-assay in three replicates. The assay CV values are reliable ranges of 0.6%–6.9% at higher MFI and 0.9%–9.7% at middle MFI. The assay reliability around LLOQ decreased reliability CVs for 2.0%–60.1% in range. However, these CV values improved to be less than 20% when the MFI signals use only more than 100 (low 0.4% of full range). Thus, intra-assay validation demonstrated a highly reliable MUSCAT-assay system showing CV less than 20% by adjusting the LLOQ value.

I evaluated the precision of the inter-assay by setting the same sample assay on different days. The assay precision is classified into three groups CV≦20%, 20%<CV≦30%, and CV>30% are 20, 17, and 22 antigens, respectively. These CV values can improve by using MFI signals more than 100; CV≦20%, 20%<CV≦30%, and CV>30% are 44, 11, and 4 antigens, respectively (Table 2-3B).

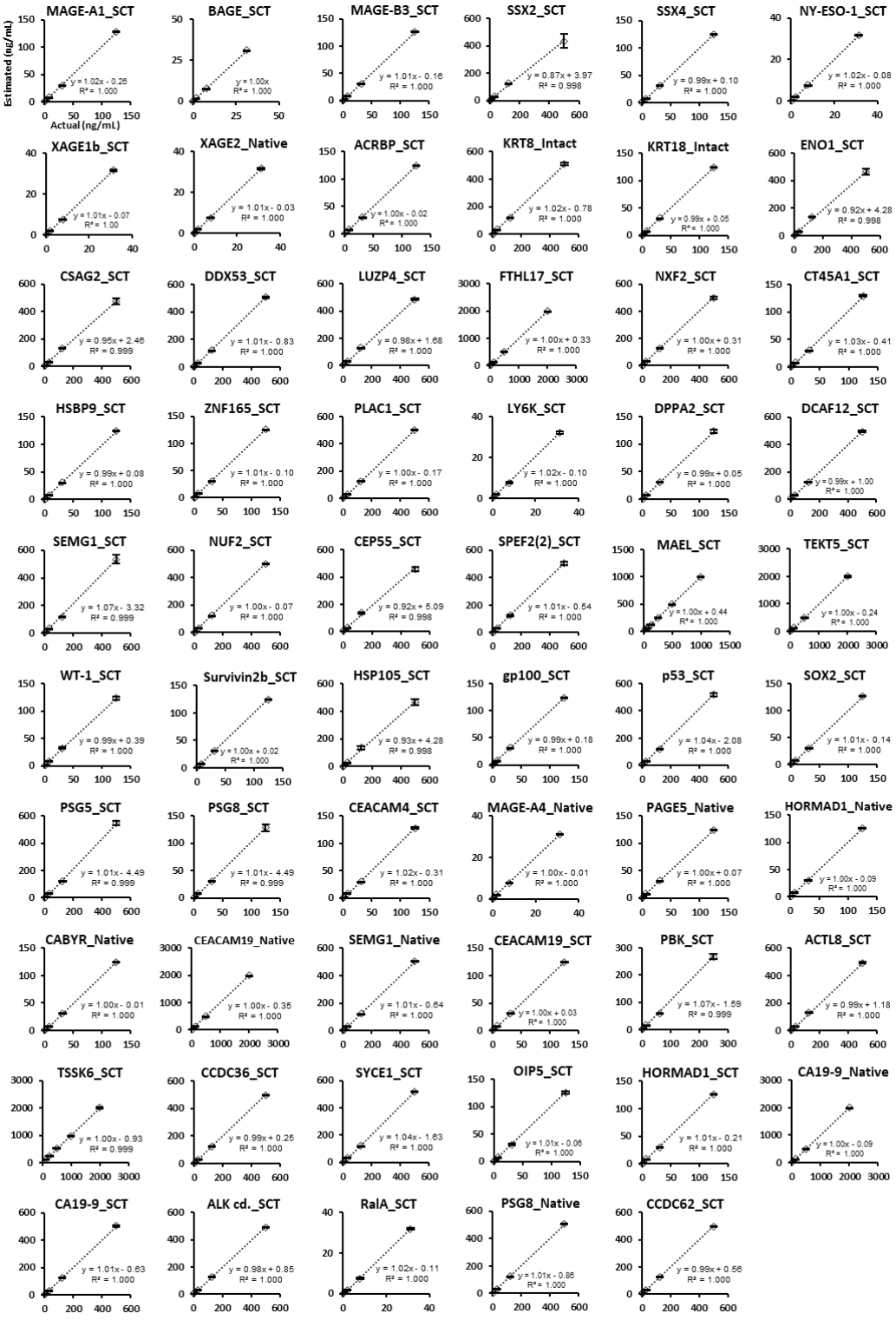

Figure 2-2 Linearity of dilution in control antibodies (n=3).

The correlation between the antibody concentration estimated from each regression curve and the actual concentration was evaluated. The estimated and actual sample concentrations within the dynamic range were plotted and correlation coefficient (R^2) values were determined by linear regression analysis.

Table 2-3　Dynamic range and precision in antigen immobilized bead validation.

A　Dynamic range and intra-assay in antigen immobilized bead validation.

No.	Control rabbit pAb	Dynamic range	Intra-asssay(n=3)							
			Low signal		Low signal(100≧)		Middle signal		High signal	
		ng/mL	MFI	CV(%)	MFI	CV(%)	MFI	CV(%)	MFI	CV(%)
1	MAGE-A1_SCT	0.49 - 125	42.9	9.6	333.7	4.4	6899.8	2.2	21000.3	1.4
2	BAGE_SCT	0.12 - 31.3	26.2	34.3	177.3	8.8	4823.9	4.1	18941.7	3.4
3	MAGE-B3_SCT	0.49- 125	24.5	26.9	177.3	5.1	4518.3	6.2	17942.6	2.4
4	SSX2_SCT	1.95 - 500	82.8	11.0	762.4	3.4	14742.5	2.7	24227.8	1.5
5	SSX4_SCT	0.49 - 125	86.2	12.3	554.0	4.2	10741.5	2.0	25164.7	2.2
6	NY-ESO-1_SCT	0.49 - 31.3	52.8	15.6	527.0	6.5	2923.8	5.1	12213.9	3.7
7	XAGE-1b_SCT	0.49 - 31.3	175.5	8.4	175.5	8.4	4148.7	9.7	16455.3	7.4
8	XAGE2_Native	0.12 - 31.3	23.6	23.6	177.8	9.5	4107.6	7.2	17286.2	3.2
9	ACRBP_SCT	1.95 - 125	61.9	24.4	514.6	20.2	3110.4	4.7	13103.8	3.8
10	KRT8_Intact	1.95 - 500	35.4	17.4	189.3	13.1	5480.3	2.7	18103.1	3.2
11	KRT18_Intact	0.49 - 125	46.8	32.4	409.2	8.1	12747.2	4.1	23643.9	3.1
12	ENO1_SCT	1.95 - 500	125.3	9.2	125.3	9.2	5966.8	3.0	24476.4	1.7
13	CSAG2_SCT	1.95 - 500	52.3	19.5	477.8	6.9	10385.8	2.6	23702.8	0.6
14	DDX53_SCT	1.95 - 500	29.3	9.8	309.5	5.1	8481.5	3.6	22111.7	3.0
15	LUZP4_SCT	1.95 - 500	80.8	16.6	748.7	9.0	13997.2	4.6	23961.7	0.7
16	FTHL17_SCT	7.81 - 2000	25.3	13.3	162.1	6.3	4735.2	7.7	11579.8	5.4
17	NXF2_SCT	1.95 - 500	84.3	25.5	634.3	5.2	11122.1	3.9	20854.6	1.3
18	CT45A1_SCT	0.49 - 125	49.3	13.5	375.0	5.5	9646.3	1.1	24080.3	1.3
19	HSPB9_SCT	0.49 - 125	84.4	9.7	468.2	6.8	8903.8	4.0	23307.1	1.6
20	ZNF165_SCT	0.49 - 125	23.3	13.1	193.6	6.4	4435.3	0.9	16590.4	1.0
21	PLAC1_SCT	1.95 - 500	54.9	8.3	451.6	7.3	8540.2	7.4	23660.5	0.6
22	LY6K_SCT	0.49 - 31.3	82.2	13.0	650.3	6.1	3174.2	5.6	11761.8	6.2
23	DPPA2_SCT	1.95 - 125	57.0	16.6	421.8	2.3	2080.9	4.1	8235.5	1.6
24	DCAF12_SCT	7.81 - 500	47.5	10.2	365.8	15.4	2544.7	2.8	9488.6	3.2
25	SEMG1_SCT	1.95 - 500	20.3	47.5	122.2	9.0	4711.4	6.5	16724.8	2.3
26	NUF2_SCT	1.95 - 500	52.2	16.4	370.2	10.7	9695.3	1.5	24147.8	0.8
27	CEP55_SCT	1.95 - 500	102.1	11.1	102.1	11.1	4984.1	5.0	25808.4	3.3
28	SPEF2(2)_SCT	1.95 - 500	41.9	9.2	395.6	6.2	8590.6	7.5	20876.3	3.9
29	MAEL_SCT	31.3 - 1000	12.0	35.7	102.1	17.8	644.0	6.0	1095.2	5.4
30	TEKT5_SCT	7.81 - 2000	41.3	11.1	345.5	6.7	8797.7	5.2	19393.6	5.8
31	WT-1_SCT	1.95 - 125	125.2	8.5	640.6	2.8	2941.1	9.9	10324.1	2.8
32	Survivin2b_SCT	1.95 - 125	199.9	2.0	199.9	2.0	7357.7	4.8	22849.4	1.4
33	HSP105_SCT	1.95 - 500	140.6	16.9	140.6	16.9	15424.2	4.2	24355.8	1.1
34	gp100_SCT	0.49 - 125	69.7	8.9	545.3	5.3	12103.0	3.2	26391.6	1.9
35	p53_SCT	1.95 - 500	41.8	10.4	276.0	4.7	4647.0	3.1	13554.3	5.3
36	SOX2_SCT	0.49 - 125	47.4	20.1	245.5	11.8	5238.5	4.3	19105.8	2.7
37	PSG5_SCT	1.95 - 500	30.3	17.1	296.2	3.8	8453.5	3.9	21042.3	4.0
38	PSG8_SCT	1.95 - 125	126.2	8.7	126.2	8.7	7064.1	4.8	23478.9	3.1
39	CEACAM4_SCT	0.49 - 125	10.1	59.4	701.1	5.0	3753.2	3.4	14989.3	6.2
40	MAGE-A4_Native	0.49 - 31.3	85.3	8.2	598.5	2.2	3341.3	5.3	16957.7	7.9
41	PAGE5_Native	0.49 - 125	71.6	7.7	527.3	10.4	10509.3	3.9	23925.3	1.5
42	HORMAD1_Native	1.95 - 125	190.0	18.3	190.0	18.3	4706.8	3.8	18994.9	4.7
43	CABYR_Native	0.49 - 125	19.2	19.3	200.5	9.4	7482.7	3.6	24908.8	2.7
44	CEACAM19_Native	31.3 - 2000	15.3	53.8	104.9	9.0	619.8	7.2	1772.3	3.7
45	SEMG1_Native	1.95 - 500	42.3	14.7	243.3	8.2	6052.3	3.6	20299.3	2.7
46	CEACAM19_SCT	0.49 - 125	202.1	13.8	202.1	13.8	10745.3	5.9	23530.3	1.1
47	PBK_SCT	0.98 - 250	12.9	60.1	177.3	5.6	7218.6	4.0	22031.5	3.7
48	ACTL8_SCT	1.95 - 500	72.8	32.1	622.4	6.3	12705.4	5.8	24528.7	6.1
49	TSSK6_SCT	125 - 2000	76.1	8.9	216.0	8.9	1252.8	4.2	2230.9	6.4
50	CCDC36_SCT	1.95 - 500	88.2	22.6	558.0	5.0	10865.2	2.5	23578.4	1.3
51	SYCE1_SCT	1.95 - 500	25.3	36.9	202.8	5.0	6451.8	3.5	20971.3	4.1
52	OIP5_SCT	0.49 - 125	34.3	40.7	341.2	8.9	7647.8	6.7	22474.9	4.0
53	HORMAD1_SCT	0.49 - 125	36.3	24.9	225.4	4.6	6024.8	2.5	22321.3	5.6
54	CA19-9_Native	31.3 - 2000	59.0	8.6	450.8	3.2	2806.9	2.3	10035.2	4.3
55	CA19-9_SCT	1.95 - 500	59.3	20.2	383.1	6.1	9056.3	5.2	23735.8	1.2
56	ALK.cd_SCT	1.95 - 500	134.8	10.7	134.8	3.6	14231.9	2.7	24179.2	6.9
57	RalA_SCT	0.12 - 31.3	77.7	14.1	353.3	2.2	4655.6	3.7	17329.0	3.3
58	PSG8_Native	7.81 - 500	94.0	9.6	753.3	3.4	3810.7	1.6	11062.7	2.4
59	CCDC62_SCT	1.95 - 500	51.0	20.2	420.3	15.3	11747.6	5.7	23617.3	0.6

Table 2-3 Cont.

B Inter-assay in antigen immobilized bead validation.

No.	Control rabbit pAb	Inter-asssay(n=3, 2days)							
		Low signal		Low signal(100≧)		Meddle signal		High signal	
		MFI	CV(%)	MFI	CV(%)	MFI	CV(%)	MFI	CV(%)
1	MAGE-A1_SCT	42.9	12.2	333.7	8.9	6899.8	10.4	21000.3	7.8
2	BAGE_SCT	26.2	39.8	177.3	19.1	4823.9	4.1	18941.7	4.1
3	MAGE-B3_SCT	24.5	32.2	177.3	6.8	4518.3	11.3	17942.6	6.2
4	SSX2_SCT	82.8	16.0	762.4	4.4	14742.5	6.5	24227.8	2.0
5	SSX4_SCT	86.2	17.9	554.0	8.0	10741.5	2.0	25164.7	4.1
6	NY-ESO-1_SCT	52.8	16.0	527.0	9.4	2923.8	5.1	12213.9	3.8
7	XAGE-1b_SCT	175.5	8.4	175.5	8.4	4148.7	9.7	16455.3	7.4
8	XAGE2_Native	23.6	23.6	177.8	9.5	4107.6	7.2	17286.2	3.2
9	ACRBP_SCT	61.9	32.8	514.6	25.1	3110.4	7.2	13103.8	3.9
10	KRT8_Intact	35.4	23.3	189.3	17.3	5480.3	8.6	18103.1	11.7
11	KRT18_Intact	46.8	43.1	409.2	8.7	12747.2	7.5	23643.9	3.6
12	ENO1_SCT	125.3	22.3	125.3	22.3	5966.8	8.0	24476.4	3.7
13	CSAG2_SCT	52.3	39.8	477.8	24.7	10385.8	18.3	23702.8	1.2
14	DDX53_SCT	29.3	48.5	309.5	14.7	8481.5	4.4	22111.7	7.6
15	LUZP4_SCT	80.8	19.5	748.7	9.9	13997.2	6.3	23961.7	1.3
16	FTHL17_SCT	25.3	23.9	162.1	14.9	4735.2	9.0	11579.8	7.3
17	NXF2_SCT	84.3	38.7	634.3	12.1	11122.1	7.7	20854.6	10.6
18	CT45A1_SCT	49.3	37.0	375.0	22.7	9646.3	8.1	24080.3	1.4
19	HSPB9_SCT	84.4	17.5	468.2	9.3	8903.8	7.2	23307.1	1.7
20	ZNF165_SCT	23.3	15.0	193.6	15.6	4435.3	8.9	16590.4	8.5
21	PLAC1_SCT	54.9	39.0	451.6	26.2	8540.2	16.2	23660.5	1.4
22	LY6K_SCT	82.2	19.5	650.3	7.9	3174.2	12.3	11761.8	7.0
23	DPPA2_SCT	57.0	25.1	421.8	6.9	2080.9	8.3	8235.5	9.5
24	DCAF12_SCT	47.5	22.0	365.8	19.7	2544.7	7.0	9488.6	4.1
25	SEMG1_SCT	20.3	53.2	122.2	12.6	4711.4	8.6	16724.8	5.3
26	NUF2_SCT	52.2	27.2	370.2	10.8	9695.3	7.2	24147.8	0.9
27	CEP55_SCT	102.1	28.8	102.1	28.8	4984.1	11.4	25808.4	4.0
28	SPEF2(2)_SCT	41.9	10.8	395.6	6.4	8590.6	9.0	20876.3	4.9
29	MAEL_SCT	12.0	48.1	102.1	21.1	644.0	22.1	1095.2	14.5
30	TEKT5_SCT	41.3	22.9	345.5	15.0	8797.7	13.3	19393.6	12.8
31	WT-1_SCT	125.2	26.1	640.6	6.0	2941.1	10.3	10324.1	6.3
32	Survivin2b_SCT	199.9	9.7	199.9	9.7	7357.7	5.0	22849.4	2.2
33	HSP105_SCT	140.6	22.1	140.6	22.1	15424.2	9.0	24355.8	1.6
34	gp100_SCT	69.7	26.2	545.3	16.1	12103.0	14.0	26391.6	9.4
35	p53_SCT	41.8	13.3	276.0	12.0	4647.0	6.8	13554.3	6.5
36	SOX2_SCT	47.4	23.4	245.5	14.1	5238.5	7.1	19105.8	4.3
37	PSG5_SCT	30.3	43.1	296.2	19.5	8453.5	16.1	21042.3	14.7
38	PSG8_SCT	126.2	9.5	126.2	9.5	7064.1	6.9	23478.9	4.6
39	CEACAM4_SCT	10.1	59.6	701.1	6.8	3753.2	4.4	14989.3	8.3
40	MAGE-A4_Native	85.3	17.2	598.5	5.8	3341.3	6.3	16957.7	12.9
41	PAGE5_Native	71.6	12.0	527.3	11.8	10509.3	8.9	23925.3	1.7
42	HORMAD1_Native	190.0	37.8	190.0	37.8	4706.8	8.4	18994.9	8.2
43	CABYR_Native	19.2	22.9	200.5	9.9	7482.7	5.2	24908.8	4.8
44	CEACAM19_Native	15.3	54.6	104.9	13.9	619.8	15.4	1772.3	9.7
45	SEMG1_Native	42.3	24.2	243.3	23.6	6052.3	14.4	20299.3	14.1
46	CEACAM19_SCT	202.1	39.1	202.1	39.1	10745.3	6.9	23530.3	1.2
47	PBK_SCT	12.9	79.2	177.3	5.9	7218.6	5.6	22031.5	5.6
48	ACTL8_SCT	72.8	37.8	622.4	12.8	12705.4	7.7	24528.7	7.8
49	TSSK6_SCT	76.1	10.4	216.0	11.9	1252.8	4.4	2230.9	7.8
50	CCDC36_SCT	88.2	37.0	558.0	12.6	10865.2	10.7	23578.4	1.7
51	SYCE1_SCT	25.3	60.2	202.8	5.7	6451.8	3.7	20971.3	5.3
52	OIP5_SCT	34.3	49.6	341.2	30.3	7647.8	12.4	22474.9	6.4
53	HORMAD1_SCT	36.3	29.9	225.4	5.5	6024.8	3.4	22321.3	5.7
54	CA19-9_Native	59.0	24.8	450.8	21.0	2806.9	19.2	10035.2	9.8
55	CA19-9_SCT	59.3	28.9	383.1	11.4	9056.3	6.1	23735.8	1.5
56	ALK.cd_SCT	134.8	14.2	134.8	14.2	14231.9	6.7	24179.2	8.8
57	RalA_SCT	77.7	28.1	353.3	16.1	4655.6	4.0	17329.0	3.9
58	PSG8_Native	94.0	11.1	753.3	5.8	3810.7	4.5	11062.7	3.2
59	CCDC62_SCT	51.0	30.1	420.3	19.3	11747.6	6.6	23617.3	1.8

The quality of antigen-immobilized Luminex beads was verified by 59 different antigen-specific purified rabbit polyclonal antibodies**. (A)**MFI and CV are based on the average of two independent assays. **(B)** MFI is based on the average of two independent assays.

Assay validation by human healthy donor samples

The assay precision toward 119-antigens immobilized beads was evaluated by human-derived plasma from 120 healthy donors with non-tumor and non-autoimmunity clinical history. The assay precision was almost comparable for that demonstrated by 59 of rabbit-derived control antibodies (Table 2-4). The inter-assay CV values are 0.2%–46.8% (Excluding CA19-9 Native and CEACAM19 Native, which contain MFI less than 0). However, these CV values improved to be less than 20% when the MFI signals use only more than 100. As for the inter-assay precision, CV≦20% and 20%<CV≦30% are 59 and 6 antigens, respectively, when MFI signals more than 100 (65 antigens).

Antigen and antigen-immobilized bead batch reproducibility

The reproducibility was evaluated about recombinant protein expression, purification of *S*-cationized antigens, and immobilization of antigens onto Luminex beads on three different batches of p53 protein. As for *S*-cationized antigen preparations, chromatographic elution profiles, sharpness of peak fractions, and retention times were comparable on the reversed-phase HPLC in three bathes (Figure 2-3A). The reproducibility of MUSCAT-assay signals was evaluated by using p53 immobilized beads prepared by three other batches of antigen conjugated at the same time (Figure 2-3B) and the same antigens conjugated at different days (Figure 2-3C). The antigen preparation batch depended on CVs was 0.8%–4.2%, and the antigen conjugation bach depended on CVs was 6.5%–13.3%. Thus, this MUSCAT-assay beads preparation reproducibility is high enough to achieve CVs with less than 20% accuracy.

Table 2-4 Assay validation

No.	Antigen-immobilized bead	MFI	%CV		No.	antigen-immobilized bead	MFI	%CV	
			Intra-assay	Intre-assay				Intra-assay	Intre-assay
1	A1AT_Native	11.3	22.2	34.7	61	RalA_SCT	171.8	9.3	16.2
2	A1AT_SCT	69	7.8	8.0	62	RhoGDI_Native	33.3	5.5	10.1
3	A2B1_Native	379.2	2.9	3.4	63	RhoGDI_SCT	66.2	7.5	14.5
4	A2B1_SCT	109.7	3.4	5.2	64	SOX2_SCT	66.5	9.7	11.4
5	AARS_SCT	234	0.5	1.5	65	Survivin2b_SCT	102.5	7.0	24.3
6	EEF1A1_SCT	24.1	9.3	13.3	66	TCP1_SCT	107.4	2.6	6.1
7	EEF1G_SCT	1324.8	1.8	2.0	67	WT-1_SCT	383.8	6.3	6.6
8	EEF2K_SCT	165.4	5.3	14.1	68	ACRBP_SCT	1518.4	6.0	7.3
9	FKBP4_Native	176.8	4.0	8.3	69	ACTL8_SCT	221	3.8	18.6
10	HARS_SCT	40.8	5.9	7.2	70	BAGE_SCT	338.9	8.1	9.0
11	HNRNPR_Native	3299.6	2.5	6.6	71	BORIS_SCT	88.1	9.1	11.3
12	HNRNPR_SCT	1524.4	1.6	2.2	72	CABYR_Native	1204.5	3.5	3.6
13	KRT18_Intact	415.3	2.6	2.7	73	CCDC36_SCT	29.8	6.9	26.5
14	KRT8_Intact	1422.3	5.9	13.8	74	CCDC62_SCT	153.5	11.2	14.7
15	LMNA_SCT	57.9	7.1	16.8	75	CEP55_SCT	147	5.9	6.2
16	PCNA_SCT	259	3.5	4.3	76	CSAG2_SCT	88.1	4.6	12.7
17	PRDX2_Native	769.8	2.4	12.1	77	CT156_SCT	42.8	4.2	16.3
18	PRDX2_SCT	117.8	3.2	5.9	78	CT45A1_SCT	864.9	5.9	14.0
19	RO52_SCT	86.6	3.6	10.4	79	Cxorf61_SCT	303	1.0	1.6
20	RO60_SCT	123.3	5.4	6.7	80	DCAF12_SCT	86.3	4.5	6.3
21	RPL7A_SCT	48.8	10.0	13.5	81	DDX53_SCT	30	20.3	26.8
22	TKT_SCT	182.9	3.0	8.5	82	DPPA2_SCT	33.8	5.9	14.0
23	TPI1_Native	283.2	3.2	7.5	83	FTHL17_SCT	115.3	6.5	10.3
24	TPI1_SCT	121	1.8	4.9	85	HORMAD1_Native	159.3	3.4	10.5
25	Vim_SCT	219	6.1	22.2	85	HORMAD1_SCT	80.8	12.8	16.1
26	Wdr36_SCT	84.9	2.2	9.6	86	HSPB9_SCT	39.5	8.8	10.5
27	AFP_Native	11.9	18.8	30.1	87	LUZP4_SCT	134.5	5.1	22.3
28	AFP_SCT	23.3	3.3	3.6	88	LY6K_SCT	163.7	3.3	19.9
29	CA125_Native	10.6	31.6	36.4	89	MAEL_SCT	1128.9	2.7	3.6
30	CA125_SCT	630.1	0.2	3.5	90	MAGE-A1_SCT	678	1.1	4.0
31	CA19-9_Native	6.2	8.2	102.6	91	MAGE-A4_Native	4424.8	4.5	7.7
32	CA19-9_SCT	186	3.1	3.9	92	MAGE-A6_Native	6404.2	2.1	2.6
33	CEA_Native	6.7	46.8	83.9	93	MAGE-B3_SCT	4774.3	5.3	11.6
34	CEA_SCT	36	7.2	8.8	94	MAGE-A3_Native	94.4	1.5	6.9
35	CYFRA_SCT	280.4	4.0	7.2	95	MAGE-C1_Native	627.6	1.2	4.4
36	SCC_Native	37.7	9.6	22.1	96	MAGE-C2_Native	3344.5	1.3	11.5
37	ALK.cd_SCT	41.5	8.2	9.2	97	MORC1_SCT	75.9	7.9	14.7
38	ANXA1_Native	116.7	5.1	6.2	98	NUF2_SCT	152.6	2.2	22.5
39	ANXA1_SCT	49.5	3.0	4.7	99	NXF2_SCT	90.3	5.1	17.7
40	CCNB1_SCT	838.7	4.4	29.0	100	NY-ESO-1_SCT	602	0.7	1.9
41	CEACAM19_Native	4.2	100.0	162.4	101	OIP5_SCT	417.3	5.4	19.8
42	CEACAM19_SCT	149.5	4.0	6.6	102	PAGE5_Native	77	9.9	15.3
43	CEACAM4_SCT	226.3	5.2	5.7	103	PBK_SCT	87.9	4.2	19.6
44	EMD_SCT	118.5	3.2	11.9	104	PLAC1_SCT	252.6	2.1	3.2
45	ENO1_SCT	91	4.3	7.0	105	SEMG1_Native	25.4	13.6	15.0
46	EZR_Native	204.9	7.0	9.7	106	SEMG1_SCT	49.6	8.0	28.9
47	EZR_SCT	42.4	6.2	19.4	107	SPA17_Native	91.1	6.3	21.5
48	gp100_SCT	119.5	3.5	6.7	108	SPNAXD_SCT	19.1	9.8	9.8
49	Her2-ECD_Native	46.5	9.2	9.7	109	SPEF2(2)_SCT	19.3	10.9	15.4
50	HSP105_SCT	870.7	1.6	4.5	110	SSX2_SCT	940.1	0.5	26.4
51	MSLN_Native	22.5	12.2	22.6	111	SSX4_SCT	61.9	4.3	15.3
52	NPM1_Native	74.7	4.4	6.1	112	SYCE1_SCT	700.5	5.4	7.0
53	NPM1_SCT	75.6	7.7	11.1	113	SYCP1_SCT	116.2	3.3	5.6
54	p53_SCT	1080.4	2.7	5.8	114	TEKT5_SCT	64.4	4.2	12.2
55	PDZD11_SCT	104.3	9.1	10.0	115	TFDP3_SCT	31.8	10.2	22.3
56	PPIB_Native	53.9	4.9	9.1	116	TSSK6_SCT	163.1	2.9	3.1
57	PPP1CA_SCT	126.8	5.3	16.0	117	XAGE-1b_SCT	55.7	4.4	12.9
58	PSG5_SCT	25.6	15.1	29.7	118	XAGE2_Native	641.3	6.2	12.6
59	PSG8_Native	6	26.3	55.5	119	ZNF165_SCT	51.2	10.4	26.0
60	PSG8_SCT	417.8	1.8	3.3					

The results of one representative person (healthy donors, 28-year-old female) are shown.

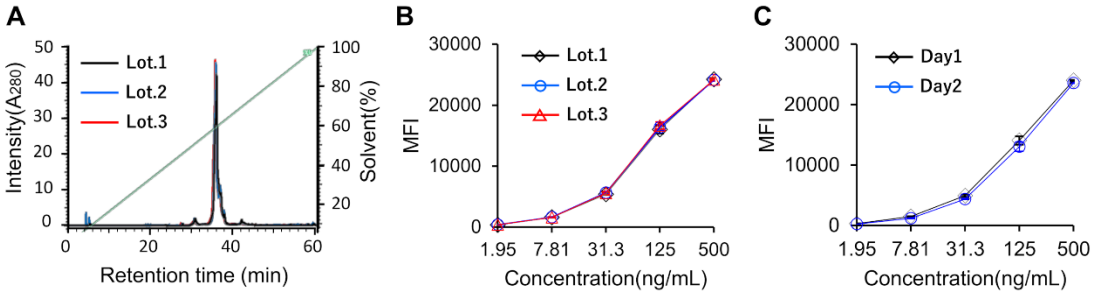

Figure 2-3 Antigen and antigen-immobilized bead batch reproducibility of p53 protein.

(A) The reproducibility of the purification of *S*-cationized antigen was evaluated using reversed-phase HPLC. This is the result of overlaid chromatograms of three lots. **(B)** The reproducibility of MUSCAT-assay signals was evaluated using p53-immobilized beads prepared by three different Lots of p53 protein conjugated at the same time. For each Lot (Lot.1-Lot.3), the mean and standard deviation (error bar) of the MFI of the three replicates at positive control antibody dilution point were plotted. **(C)** The reproducibility of MUSCAT-assay signals was evaluated using p53-immobilized beads prepared by the same Lot of p53 protein conjugated at different days. For each bead (Day1 and Day2), the mean and standard deviation (error bars) of the MFI for the three replicates at the positive control antibody dilution point were plotted.

Comparison of autoantibody distribution between NSCLC and healthy donor

The autoantibody profile in 120 healthy donors and 162 NSCLC patients was compared and showed higher autoantibody in NSCLC (Figure 2-4). For example, autoantibodies for XAGE1b, p53, and RO52 showed distinctly higher levels in NSCLC. Because antigens for CTAs and TAAs are known to express higher or discriminatory in tumors but not in normal tissues, autoantibodies to CTAs/TAAs in NSCLCs suggest the result of antitumor immune reactions. Those for healthy donors may tell a history of natural tumor rejection or immunity against pretumor cells. Higher levels of autoantibodies to autoimmunity-related antigens in NSCLC are insightful to show a close relation between antitumor immunity and autoimmunity.

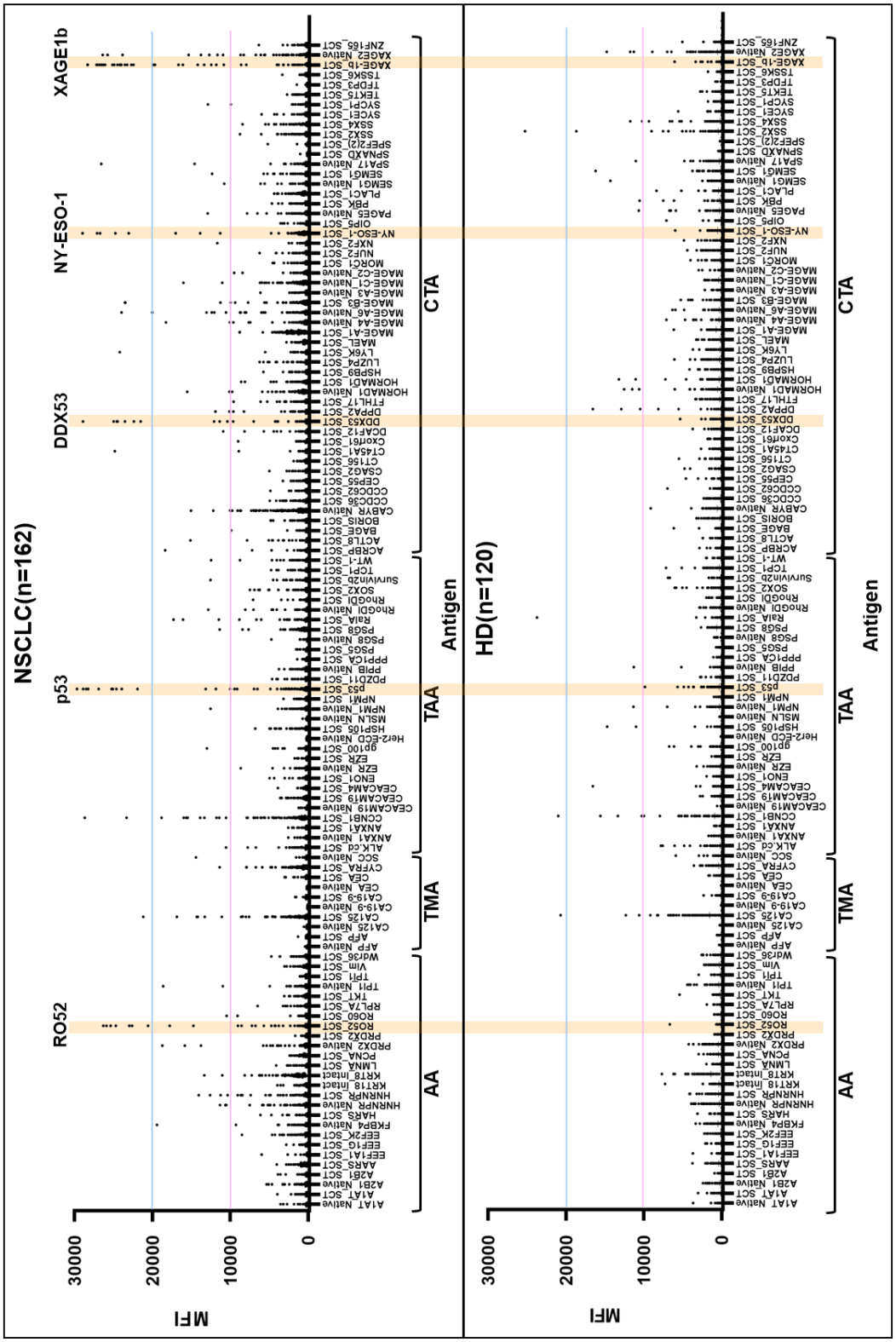

Figure 2-4 Autoantibodies are higher in NSCLC than in healthy donors.

Results of 118 antibody titers in 162 NSCLC patients and 120 HD patients were plotted to compare patterns of autoantibody appearance. AA, autoimmune disease-associated antigen; TMA, tumor marker antigen; TAA, tumor-associated antigen; CTA, cancer/testis antigen.

Discussion

Autoantibody biomarkers reflect the autoimmune reactions and elimination of tumor cells by antitumor immune responses. Because antitumor immune response and antitumor immune reactions are closely related, both antigens were selected on the MUSCAT-assay panel. Antibodies have five immunoglobulin classes (isotypes) IgG, IgM, IgA, IgE, and IgD. The secondary antibodies can select the detection of isotypes, and IgG requiring B-cell stimulation by their target antigens for their maturation was chosen as a biomarker reflecting antitumor immunity in this study [48].

In this study, the MUSCAT-assay panel composed of 120 antigens showed high enough assay fidelity within CV<20% assay accuracy. The reproducibility of antigen preparation and validation system for assay satisfy the requirement for clinical use of this panel. Inter-assay accuracy requires a critical subject for the monitoring assay on clinical samples. Diagnosis tools that are non-invasive, easy to repeat use, robust, and easy to handle in every clinical site are demanded in cancer immunotherapy.

A comparison of the autoantibodies profiles between NSCLC and healthy subjects showed clear differences between the two groups. Antibodies that showed high values only in NSCLC may be important as biomarkers. In the future, the use of autoantibody assay results from healthy subjects as a reference database may improve the accuracy of predicting clinical response. This system can measure many types of autoantibodies at once, compared to the ELISA method used in blood-based biomarker studies. Thus, results that reflect the tumor microenvironment in greater detail may be obtained.

ACKNOWLEDGMENTS

I wish to express my sincere gratitude to Professor Junichiro Futami for his supervision throughout my bachelor, master's, and doctor's courses at Okayama University. Without his extraordinary understanding and cooperation, I could not be able to finish my doctoral research completely. I wish to express my sincere thanks for his kindness and encouragement throughout this study.

I would like to thank the thesis reviewing committee and co-supervisors, Professor Hiroshi Tokumitsu and Professor Toru Ide, for their valuable comments and suggestions for my thesis.

I greatly appreciate Professor Mikio Oka for providing the XAGE-1b specific monoclonal antibody (clone:USO9-13).

I greatly appreciate Professor Dr. Katsuyuki Kiura and Professor Dr. Kadoaki Ohashi for providing clinical samples (NSCLC).

I greatly appreciate all members and graduates of the Professor Futami’s laboratory for their kindness and warm hospitality. In particular, I am thankful to Assistant Professor Dr. Nobuhiro Okada and Technical Staff Tomoko Honjo for their great supports.

This work was partially supported by JST START, Grant Number JPMJST1918(JF). This work was supported by JST SPRING, Grant Number JPMJSP2126 and Science and Technology Promotion grants (2019-2021) in Okayama Prefecture, Japan.

Ai Miyamoto

REFERENCES

1. Gajewski, T.F., H. Schreiber, and Y.X. Fu, *Innate and adaptive immune cells in the tumor microenvironment.* Nat Immunol, 2013. **14**(10): p. 1014-22.
2. Jeanbart, L. and M.A. Swartz, *Engineering opportunities in cancer immunotherapy.* Proc Natl Acad Sci U S A, 2015. **112**(47): p. 14467-72.
3. Nishikawa, H. and S. Sakaguchi, *Regulatory T cells in cancer immunotherapy.* Curr Opin Immunol, 2014. **27**: p. 1-7.
4. Schreiber, R.D., L.J. Old, and M.J. Smyth, *Cancer immunoediting: integrating immunity's roles in cancer suppression and promotion.* Science, 2011. **331**(6024): p. 1565-70.
5. Hoption Cann, S.A., J.P. van Netten, and C. van Netten, *Dr William Coley and tumour regression: a place in history or in the future.* Postgrad Med J, 2003. **79**(938): p. 672-80.
6. Carlson, R.D., J.C. Flickinger, and A.E. Snook, *Talkin' Toxins: From Coley's to Modern Cancer Immunotherapy.* Toxins (Basel), 2020. **12**(4).
7. Allison, K.H. and G.W. Sledge, *Heterogeneity and cancer.* Oncology (Williston Park), 2014. **28**(9): p. 772-8.
8. Wang, C., et al., *CancerTracer: a curated database for intrapatient tumor heterogeneity.* Nucleic Acids Res, 2020. **48**(D1): p. D797-D806.
9. Aptsiauri, N., et al., *MHC class I antigens and immune surveillance in transformed cells.* Int Rev Cytol, 2007. **256**: p. 139-89.
10. Chen, D.S. and I. Mellman, *Oncology meets immunology: the cancer-immunity cycle.* Immunity, 2013. **39**(1): p. 1-10.
11. Cheever, M.A., et al., *The prioritization of cancer antigens: a national cancer institute pilot project for the acceleration of translational research.* Clin Cancer Res, 2009. **15**(17): p. 5323-37.
12. Scanlan, M.J., et al., *Cancer/testis antigens: an expanding family of targets for cancer immunotherapy.* Immunol Rev, 2002. **188**: p. 22-32.
13. Scanlan, M.J., A.J. Simpson, and L.J. Old, *The cancer/testis genes: review, standardization, and commentary.* Cancer Immun, 2004. **4**: p. 1.
14. Caballero, O.L. and Y.T. Chen, *Cancer/testis (CT) antigens: potential targets for immunotherapy.* Cancer Sci, 2009. **100**(11): p. 2014-21.
15. Tran, E., et al., *Cancer immunotherapy based on mutation-specific CD4+ T cells in a patient with epithelial cancer.* Science, 2014. **344**(6184): p. 641-5.
16. Yadav, M., et al., *Predicting immunogenic tumour mutations by combining mass*

spectrometry and exome sequencing. Nature, 2014. **515**(7528): p. 572-6.

17. Alexandrov, L.B., et al., *Signatures of mutational processes in human cancer.* Nature, 2013. **500**(7463): p. 415-21.
18. Ohue, Y., et al., *Antibody response to cancer/testis (CT) antigens: A prognostic marker in cancer patients.* Oncoimmunology, 2014. **3**(11): p. e970032.
19. Ohue, Y., et al., *Prolongation of overall survival in advanced lung adenocarcinoma patients with the XAGE1 (GAGED2a) antibody.* Clin Cancer Res, 2014. **20**(19): p. 5052-63.
20. Ohue, Y., et al., *Serum Antibody Against NY-ESO-1 and XAGE1 Antigens Potentially Predicts Clinical Responses to Anti-Programmed Cell Death-1 Therapy in NSCLC.* J Thorac Oncol, 2019. **14**(12): p. 2071-2083.
21. Gnjatic, S., et al., *Seromic profiling of ovarian and pancreatic cancer.* Proc Natl Acad Sci U S A, 2010. **107**(11): p. 5088-93.
22. Gottschalk, S., et al., *A vaccine that co-targets tumor cells and cancer associated fibroblasts results in enhanced antitumor activity by inducing antigen spreading.* PLoS One, 2013. **8**(12): p. e82658.
23. Nesslinger, N.J., et al., *A viral vaccine encoding prostate-specific antigen induces antigen spreading to a common set of self-proteins in prostate cancer patients.* Clin Cancer Res, 2010. **16**(15): p. 4046-56.
24. Brossart, P., *The Role of Antigen Spreading in the Efficacy of Immunotherapies.* Clin Cancer Res, 2020. **26**(17): p. 4442-4447.
25. Gupta, A., et al., *A novel human-derived antibody against NY-ESO-1 improves the efficacy of chemotherapy.* Cancer Immun, 2013. **13**: p. 3.
26. de Moel, E.C., et al., *Autoantibody Development under Treatment with Immune-Checkpoint Inhibitors.* Cancer Immunol Res, 2019. **7**(1): p. 6-11.
27. Sakai, Y., et al., *A novel automated immunoassay for serum NY-ESO-1 and XAGE1 antibodies in combinatory prediction of response to anti-programmed cell death-1 therapy in non-small-cell lung cancer.* Clin Chim Acta, 2021. **519**: p. 51-59.
28. DiLillo, D.J. and J.V. Ravetch, *Differential Fc-Receptor Engagement Drives an Anti-tumor Vaccinal Effect.* Cell, 2015. **161**(5): p. 1035-1045.
29. Ahmadi, H., et al., *Unusual aggregation property of recombinantly expressed cancer-testis antigens in mammalian cells.* J Biochem, 2021. **170**(3): p. 435-443.
30. Rajagopalan, K., et al., *A majority of the cancer/testis antigens are intrinsically disordered proteins.* J Cell Biochem, 2011. **112**(11): p. 3256-67.
31. Tompa, P. and P. Csermely, *The role of structural disorder in the function of RNA and protein chaperones.* FASEB J, 2004. **18**(11): p. 1169-75.

32. Futami, J., et al., *Sensitive Multiplexed Quantitative Analysis of Autoantibodies to Cancer Antigens with Chemically S-Cationized Full-Length and Water-Soluble Denatured Proteins.* Bioconjug Chem, 2015. **26**(10): p. 2076-84.
33. Kawabata, R., et al., *Antibody response against NY-ESO-1 in CHP-NY-ESO-1 vaccinated patients.* Int J Cancer, 2007. **120**(10): p. 2178-84.
34. Ohue, Y., et al., *Spontaneous antibody, and CD4 and CD8 T-cell responses against XAGE-1b (GAGED2a) in non-small cell lung cancer patients.* Int J Cancer, 2012. **131**(5): p. E649-58.
35. Kimura, S., K. Imamura, and J. Futami, *A suitable and effective stepwise oxidative refolding procedure for highly-cationic tetrameric avidin in nucleic acid free conditions.* Biotechnol Prog, 2020. **36**(5): p. e3031.
36. Futami, M., et al., *Enhanced in-cell folding of reversibly cationized transcription factor using amphipathic peptide.* J Biosci Bioeng, 2017. **123**(4): p. 419-424.
37. Futami, J., et al., *Evaluation of irreversible protein thermal inactivation caused by breakage of disulphide bonds using methanethiosulphonate.* Sci Rep, 2017. **7**(1): p. 12471.
38. Chen, D.S. and I. Mellman, *Elements of cancer immunity and the cancer-immune set point.* Nature, 2017. **541**(7637): p. 321-330.
39. Lee, H.T., S.H. Lee, and Y.S. Heo, *Molecular Interactions of Antibody Drugs Targeting PD-1, PD-L1, and CTLA-4 in Immuno-Oncology.* Molecules, 2019. **24**(6).
40. Lohmueller, J. and O.J. Finn, *Current modalities in cancer immunotherapy: Immunomodulatory antibodies, CARs and vaccines.* Pharmacol Ther, 2017. **178**: p. 31-47.
41. Salemme, V., et al., *The Crosstalk Between Tumor Cells and the Immune Microenvironment in Breast Cancer: Implications for Immunotherapy.* Front Oncol, 2021. **11**: p. 610303.
42. Karasaki, T., et al., *An Immunogram for the Cancer-Immunity Cycle: Towards Personalized Immunotherapy of Lung Cancer.* J Thorac Oncol, 2017. **12**(5): p. 791-803.
43. Luo, B., et al., *The role of seven autoantibodies in lung cancer diagnosis.* J Thorac Dis, 2021. **13**(6): p. 3660-3668.
44. Das, S. and D.B. Johnson, *Immune-related adverse events and anti-tumor efficacy of immune checkpoint inhibitors.* J Immunother Cancer, 2019. **7**(1): p. 306.
45. Khoja, L., et al., *Tumour- and class-specific patterns of immune-related adverse events of immune checkpoint inhibitors: a systematic review.* Ann Oncol, 2017. **28**(10): p. 2377-2385.
46. Liu, Y.T. and Z.J. Sun, *Turning cold tumors into hot tumors by improving T-cell*

infiltration. Theranostics, 2021. **11**(11): p. 5365-5386.

47. Hendriks, L.E., E. Rouleau, and B. Besse, *Clinical utility of tumor mutational burden in patients with non-small cell lung cancer treated with immunotherapy.* Transl Lung Cancer Res, 2018. **7**(6): p. 647-660.
48. Lagos, G.G., B. Izar, and N.A. Rizvi, *Beyond Tumor PD-L1: Emerging Genomic Biomarkers for Checkpoint Inhibitor Immunotherapy.* Am Soc Clin Oncol Educ Book, 2020. **40**: p. 1-11.
49. Dudley, J.C., et al., *Microsatellite Instability as a Biomarker for PD-1 Blockade.* Clin Cancer Res, 2016. **22**(4): p. 813-20.
50. Bjerre, M., et al., *Simultaneous detection of porcine cytokines by multiplex analysis: development of magnetic bioplex assay.* Vet Immunol Immunopathol, 2009. **130**(1-2): p. 53-8.
51. Ramaraj, T., et al., *Antigen-antibody interface properties: composition, residue interactions, and features of 53 non-redundant structures.* Biochim Biophys Acta, 2012. **1824**(3): p. 520-32.
52. Kumon, H., et al., *Ad-REIC Gene Therapy: Promising Results in a Patient with Metastatic CRPC Following Chemotherapy.* Clin Med Insights Oncol, 2015. **9**: p. 31-8.
53. Kumon, H., et al., *Adenovirus vector carrying REIC/DKK-3 gene: neoadjuvant intraprostatic injection for high-risk localized prostate cancer undergoing radical prostatectomy.* Cancer Gene Ther, 2016. **23**(11): p. 400-409.
54. Abarzua, F., et al., *Adenovirus-mediated overexpression of REIC/Dkk-3 selectively induces apoptosis in human prostate cancer cells through activation of c-Jun-NH2-kinase.* Cancer Res, 2005. **65**(21): p. 9617-22.
55. Sakaguchi, M., et al., *Overexpression of REIC/Dkk-3 in normal fibroblasts suppresses tumor growth via induction of interleukin-7.* J Biol Chem, 2009. **284**(21): p. 14236-44.
56. Watanabe, M., et al., *Immunological aspects of REIC/Dkk-3 in monocyte differentiation and tumor regression.* Int J Oncol, 2009. **34**(3): p. 657-63.
57. Kinoshita, R., et al., *The cysteine-rich core domain of REIC/Dkk-3 is critical for its effect on monocyte differentiation and tumor regression.* Oncol Rep, 2015. **33**(6): p. 2908-14.
58. Steinbuch, M. and R. Audran, *The isolation of IgG from mammalian sera with the aid of caprylic acid.* Arch Biochem Biophys, 1969. **134**(2): p. 279-84.
59. Griffiths, E.A., et al., *NY-ESO-1 Vaccination in Combination with Decitabine Induces Antigen-Specific T-lymphocyte Responses in Patients with Myelodysplastic Syndrome.* Clin Cancer Res, 2018. **24**(5): p. 1019-1029.
60. Sato, S., et al., *Identification of XAGE-1 isoforms: predominant expression of XAGE-1b*

in testis and tumors. Cancer Immun, 2007. **7**: p. 5.

61. Nakagawa, K., et al., *XAGE-1 expression in non-small cell lung cancer and antibody response in patients.* Clin Cancer Res, 2005. **11**(15): p. 5496-503.
62. Correia, I.R., *Stability of IgG isotypes in serum.* MAbs, 2010. **2**(3): p. 221-32.
63. Ettinger, R., et al., *IL-21 induces differentiation of human naive and memory B cells into antibody-secreting plasma cells.* J Immunol, 2005. **175**(12): p. 7867-79.
64. Chiappinelli, K.B., et al., *Combining Epigenetic and Immunotherapy to Combat Cancer.* Cancer Res, 2016. **76**(7): p. 1683-9.
65. Rosenthal, R., et al., *Neoantigen-directed immune escape in lung cancer evolution.* Nature, 2019. **567**(7749): p. 479-485.
66. Yan, X., et al., *Case Report: Low-Dose Decitabine Plus Anti-PD-1 Inhibitor Camrelizumab for Previously Treated Advanced Metastatic Non-Small Cell Lung Cancer.* Front Oncol, 2020. **10**: p. 558572.
67. Woloszynska-Read, A., et al., *Intertumor and intratumor NY-ESO-1 expression heterogeneity is associated with promoter-specific and global DNA methylation status in ovarian cancer.* Clin Cancer Res, 2008. **14**(11): p. 3283-90.
68. Remon, J., et al., *Advanced-Stage Non-Small Cell Lung Cancer: Advances in Thoracic Oncology 2018.* J Thorac Oncol, 2019. **14**(7): p. 1134-1155.
69. Smithy, J.W., D.M. Faleck, and M.A. Postow, *Facts and Hopes in Prediction, Diagnosis, and Treatment of Immune-Related Adverse Events.* Clin Cancer Res, 2022. **28**(7): p. 1250-1257.
70. Goto, Y., et al., *First-Line Pembrolizumab Monotherapy for Advanced NSCLC With Programmed Death-Ligand 1 Expression Greater Than or Equal to 50%: Real-World Study Including Older Patients in Japan.* JTO Clin Res Rep, 2022. **3**(9): p. 100397.
71. Sholl, L.M., et al., *The Promises and Challenges of Tumor Mutation Burden as an Immunotherapy Biomarker: A Perspective from the International Association for the Study of Lung Cancer Pathology Committee.* J Thorac Oncol, 2020. **15**(9): p. 1409-1424.
72. Samstein, R.M., et al., *Tumor mutational load predicts survival after immunotherapy across multiple cancer types.* Nat Genet, 2019. **51**(2): p. 202-206.
73. Bagaev, A., et al., *Conserved pan-cancer microenvironment subtypes predict response to immunotherapy.* Cancer Cell, 2021. **39**(6): p. 845-865.e7.
74. Fisher, R., L. Pusztai, and C. Swanton, *Cancer heterogeneity: implications for targeted therapeutics.* Br J Cancer, 2013. **108**(3): p. 479-85.
75. Watanabe, M., et al., *A novel gene expression system strongly enhances the anticancer effects of a REIC/Dkk-3-encoding adenoviral vector.* Oncol Rep, 2014. **31**(3): p. 1089-

95.

76. Miyamoto, A., et al., *Engineering Cancer/Testis Antigens With Reversible.* Front Oncol, 2022. **12**: p. 869393.